Superfluid turbulence in a nonuniform rectangular channel

J. F. Kafkalidis, G. Klinich III, and J. T. Tough
Department of Physics, The Ohio State University, Columbus, Ohio 43210
(Received 29 April 1994; revised manuscript received 15 August 1994)

In this detailed study of inhomogeneous superfluid turbulence created in a spatially nonuniform flow, we measure the turbulent dissipation produced by thermal counterflow in a nonuniform rectangular channel. The width of the channel increases linearly with position r along the channel length to impose a known spatial nonuniformity on the velocity in the flow direction, $V \propto \dot{Q}/r$, where $\dot{Q}$ is the heat current. Because the channel widens gradually, this divergence is weak, producing a small deviation from uniform flow. Probes embedded in the channel walls allow access to the local temperature at several positions r. We employ sensitive differential thermometry to measure the temperature difference between any two of these locations to high precision. The single turbulent state we observe is clearly the analog of the T-II state of fully developed, homogeneous turbulence present in uniform flows. Making an approximation of local uniformity, we attempt to extend the theoretical description of turbulence in uniform flows to our results by replacing the uniform velocity with the local velocity in the expression for the temperature gradient. When applied locally, the Schwarz model of homogeneous turbulence, so successful in describing the T-II state in uniform flows, has the wrong dependence on both r and $\dot{Q}$ to characterize our results. The Geurst three-fluid model, which extends to situations where a gradient is present in the line density in an otherwise uniform flow, likewise does not agree with our observations when used in the local approximation. We therefore find that even a small perturbation imposed on a uniform flow radically changes the nature of the T-II state, and the inhomogeneous T-II state we observe is markedly different from that of homogeneous turbulence. This rather surprising result points to the need for a proper theory, or direct numerical simulation, of inhomogeneous turbulence in nonuniform flow. By introducing a substantial modification to the Schwarz line density, we identify a modified line density that constitutes a three-parameter fit yielding excellent agreement with our results. Finally, we find that the transition from laminar to turbulent flow occurs at a stationary front. Observations of the location of this front as a function of $\dot{Q}$ show that the critical condition for maintaining turbulence is more consistent with a minimum line density than a critical velocity.

I. BACKGROUND AND MOTIVATION

Our picture of liquid ^{4}He at absolute zero is that of a pure superfluid of density $\rho = \rho_s$, capable only of irrotational flow, and having no viscosity. Motion of this superfluid is described by a velocity field $\mathbf{v}_s$. At finite temperatures, a gas of elementary thermal excitations is also present, which on the macroscopic level manifests itself as a normal, viscous fluid with density ρ_n. The average drift velocity of the excitations determines the velocity field $\mathbf{v}_n$ of the normal fluid component. In this two-fluid model of superfluid helium (helium II), the mass transport of the total fluid can now be described as the sum $\rho_s\mathbf{v}_s + \rho_n\mathbf{v}_n$ of these two separate motions, where ρ_s and ρ_n are functions of temperature, and the total fluid has a density $\rho = \rho_s + \rho_n$.

Being the easiest to create experimentally, thermal counterflow of superfluid helium is the type of channel flow most frequently studied. One end of the channel is open to a large reservoir of helium maintained at a constant temperature, while the other end is connected to a small chamber containing a heater. Introducing a heat current $\dot{Q}$ in the sealed end causes the normal fluid to flow toward the reservoir end at an average velocity

$$V_n = \langle \mathbf{v}_n \rangle = \frac{\dot{Q}}{\rho S T A} \ , \tag{1}$$

where S is the entropy per unit mass of fluid and $\langle\ \rangle$ denotes temporal and spatial averaging of $\mathbf{v}_n$ over the cross sectional area A of the channel. While the normal fluid convects the heat away from the sealed end, the superfluid flows in the opposite direction with average velocity V_s, in accordance with the constraint that no net mass be transferred, $\rho_n V_n + \rho_s V_s = 0$. The rate of this internal convection between the two fluid components is given by the average relative velocity $V = V_n - V_s$, where for thermal counterflow

$$V = \frac{\dot{Q}}{\rho_s S T A} \ . \tag{2}$$

Although the underlying vector fields $\mathbf{v}_s$ and $\mathbf{v}_n$ are unknown functions of position, the average relative velocity V has a simple position dependence. For a uniform channel, meaning a channel with constant cross sectional area A, the relative velocity V is constant everywhere in the channel, at least as long as the overall temperature variation over the length of the channel is small enough that $\rho_s S T$ remains essentially constant throughout the

channel. In a nonuniform channel, A varies and therefore V becomes a function of position along the channel length.

At low relative velocities the flow is laminar and the viscous dissipation creates a laminar temperature gradient ∇T_L in the fluid. At a large enough relative velocity V the fluid enters a new dynamical state characterized by a dense, random tangle of quantized vortex lines in the superfluid. The mutual friction of the normal fluid excitations scattering off the vortex cores creates additional dissipation manifested as a large, nonlinear temperature gradient $\nabla T'$. This state of superfluid turbulence was first described by Vinen in terms of the amount of vortex line length per unit volume, called the line density L, where $\nabla T'$ is proportional to both L and V.[1]

Over the years, extensive experiments have been conducted in uniform channels of many cross sectional shapes and aspect ratios and a wide range of overall sizes. As well as thermal counterflow, more general flows with all possible combinations of $\mathbf{v}_n$ and $\mathbf{v}_s$ have also been studied. For such flows in uniform channels, V is still constant throughout the channel, but is no longer given by Eq. (2). Several distinct turbulent states are observed in uniform channels under these various conditions.[2,3]

Limiting our attention to thermal counterflow, a state of fully developed turbulence known as the T-II state is observed in uniform channels of either circular or rectangular cross section at high enough relative velocities. Ion trapping experiments have been successful in probing L to a 1-mm accuracy in large rectangular channels with a width of 1 cm, confirming that the T-II state is spatially homogeneous to within 1 mm of the channel walls.[4] The T-II state is modeled accurately by the theory of homogeneous superfluid turbulence developed by Schwarz.[5] Starting with an equation of motion describing the appropriate dynamics for a vortex line element, including mutual friction, Schwarz computes by direct numerical simulation the final steady-state of an initially small, arbitrary arrangement of vortex lines evolving under the influence of a uniform driving velocity V. In either the Vinen or Schwarz formalism, this theory of homogeneous turbulence predicts the steady state line density L as a function of V, and how the mutual friction yielding the temperature gradient $\nabla T'$ depends on L and V. In contrast with the earlier Vinen model, all parameters characterizing the predicted turbulent state are computed within the Schwarz model; none are adjustable. The predictions of the Schwarz model are in very good quantitative agreement with the observed T-II state in uniform channels. This state of fully developed, homogeneous turbulence is thus fairly well understood.

In uniform channels of certain geometries at more moderate relative velocities, the T-II state is preceded by another turbulent state, known as the T-I state, with a much lower line density than would be characteristic of the T-II state at the same V. This lower level of turbulence has only been observed in channels of fairly small circular and low-aspect-ratio rectangular (square) cross section, and is conspicuously absent from high-aspect-ratio rectangular channels. Schwarz and Rozen recently conjectured that the anomalous T-I state may be a state of inhomogeneous turbulence which represents a "spatially patchy precursor" to the fully developed, homogeneous T-II state.[6] Another long-standing speculation holds that spatial inhomogeneity in the turbulence could also result from a nonuniform cross-channel profile in the normal fluid velocity. Several difficulties arise in trying to determine whether the T-I state is actually one of inhomogeneous turbulence. First, the cross-channel $\mathbf{v}_n$ profile cannot be measured directly in such small channels; nor has it been predicted theoretically in the presence of the vortex tangle. In laminar flow, the $\mathbf{v}_n$ profile is computed easily enough by treating the normal fluid as an incompressible, viscous fluid and applying the appropriate boundary conditions; however, once vortex lines are present, the $\mathbf{v}_n$ profile is also influenced by their frictional interaction with the normal fluid, in a way that is not well understood and cannot presently be modeled. Second, it is equally difficult to observe any resulting spatial inhomogeneity in L in the T-I state. Channels in which the T-I state has been observed range in diameter from only 100 μm up to about 1 mm, well under the limit of resolution for an ion trapping experiment.

Once L becomes large enough, the presence of such a dense vortex tangle presumably influences the normal fluid velocity profile so significantly that any cross-channel spatial variation in $\mathbf{v}_n$ is obliterated. If so, the T-II state would thus conform to the condition of uniform relative velocity assumed in the Schwarz model of homogeneous turbulence. This scenario suggests a reason behind the transition from the T-I to the T-II state, but does nothing to predict the value of the relative velocity at which this transition occurs. Why the T-I state is not observed in rectangular channels is also unclear. One possibility is that the T-I state does in fact exist in rectangular channels, but over such a narrow range of velocities that its presence before the onset of the T-II state is indiscernible. The lack of axial symmetry in the rectangular channel flow may also play a role, making $\mathbf{v}_n$ renormalize to a flat profile more readily in this geometry.

The idea that inhomogeneous turbulence could be the result of a spatially nonuniform normal fluid velocity field provided one impetus for the present work. Our experiment was designed to study the effect on homogeneous superfluid turbulence of a small but well-controlled deviation from a spatially uniform driving velocity. Any cross-channel variations in the local relative velocity $\mathbf{v}_n - \mathbf{v}_s$ cannot be controlled, but by constructing a channel which opens up gradually along its length, the average relative velocity V can be varied in a known way along the channel length. The primary question explored in this research is whether the character of the T-II state would remain largely unaffected or be radically altered by this small perturbation imposed on a uniform flow.

We used a channel of high-aspect-ratio rectangular cross section because we wanted to isolate the influence of a nonuniform velocity on homogeneous turbulence from any ambiguity introduced by the presence of the T-I state. Moreover, we wanted to measure the temperature of the helium at several positions along the length of the channel, not just at the channel ends, in order to map out the position dependence of the temperature gradient.

For simplicity, we also wanted the cross sectional area to vary in a precisely controlled and well-defined manner. A rectangular channel could be constructed by machining, permitting both exact control of the channel shape and easy incorporation of local temperature probes. An analogous set of experiments conducted by Murphy, Castiglione, and Tough uses a flaring circular channel made from drawn glass tubing, in which the channel diameter could not be as precisely controlled, and no temperature probes could be inserted along the channel length.[7] The width of our rectangular channel increases linearly along its length, and so the cross sectional area A increases linearly with position r down the channel. This geometry produces a small, known divergence in the downstream velocity: $V \propto \dot{Q}/r$. This experimental design emulates the radial heat transfer problem of a heated wire or cylinder immersed in a large bath of superfluid helium.

We require a valid method by which to compare our experimental results with existing theory. It seems at least plausible to expect that the turbulent state forming in a flow which is only slightly nonuniform might not differ dramatically from homogeneous turbulence. The weakness of the divergence in our nonuniform flow suggests that our data may be adequately described by applying the theory of homogeneous turbulence locally. Indeed, this approach seems the only logical recourse available in lieu of a proper theory of inhomogeneous turbulence. We make this "local uniformity approximation" as follows. First, we not only assume that the density of vortex lines $L(r)$ at any point in this weakly nonuniform flow is determined solely from the local value of the velocity $V(r)$, but further that $L(r)$ bears exactly the same functional dependence on $V(r)$ as it would have in a uniform flow at that velocity. Similarly, we assume that the turbulent temperature gradient $\nabla T'(r)$ at each point r has the same functional dependence on $L(r)$ and $V(r)$ as it would in a uniform flow at equal velocity. The resulting local $\nabla T'(r)$ predicted within the local uniformity approximation can then be integrated to obtain the temperature difference between any two positions in the channel. The local uniformity approximation is analogous to the local equilibrium approximation of kinetic theory, where the equilibrium distribution function appropriate to the local values of the system thermodynamic variables is used as a substitute at every point for the actual distribution function in a nonequilibrium state, which cannot be determined.

It is entirely possible that the local uniformity approximation will fail to describe even a weakly nonuniform turbulent flow, for any number of reasons. All the parameters predicted by the Schwarz model are computed using the homogeneous distribution of vortex lines resulting from a uniform velocity; therefore these parameters may well take on quite different values in the case of inhomogeneous turbulence, or even become spatial functions. The relation between L and V for a nonuniform flow might also differ in some fundamental way from that predicted for a uniform flow, or the dependence of $\nabla T'$ on L and V might be altered. Underlying all these possibilities is the fact that the dynamical scaling arguments at the heart of the Schwarz model are worked out under the assumption of a uniform driving velocity. The local uniformity approximation consists of thumb-tacking a prediction obtained under the guise of a uniform flow onto a situation for which the prediction might prove to be quite different. No such after-the-fact modification should necessarily be expected to properly adjust the Schwarz model of homogeneous turbulence to describe inhomogeneous turbulence. If the local uniformity approximation proves inadequate, perhaps altering the underlying scaling arguments in the Schwarz model to incorporate the symmetries of the nonuniform flow appropriately and conduct a proper simulation of the vortex dynamics is all that will be needed to extend the Schwarz description to inhomogeneous turbulence.

On the other hand, perhaps a more fundamental change in the underlying vortex dynamics will be required instead. New dynamic mechanisms which do not come into play or are not discernable in uniform flows might be needed. One recent suggestion of Schwarz along these lines seems worth further investigation.[8] In being convected from one region to another in a nonuniform flow, a vortex line, being an object which exists only as a pattern in the flow itself, is "stretched," becoming longer or shorter as the flow diverges or converges. Such a vortex stretching represents a mechanism of line length production different from that already present in a uniform flow. A new line production term might need to be incorporated in the dynamics to account for this additional vortex growth mechanism.

A suggestion of a quite different nature resides in a new hydrodynamic model of superfluid turbulence recently proposed by Geurst, which introduces the effects of a nonuniform line density explicitly by including a new term in the internal energy that depends on the gradient of L.[9–11] Because the Geurst model purports to shed light on the very situation created in our experiment, we compared its predictions to our results. Our analysis was of necessity limited to the version of the Geurst model describing a one-dimensional flow at constant velocity. Despite allowing for the possibility of inhomogeneous turbulence, this one-dimensional Geurst model could only be applied to our nonuniform flow in the local uniformity approximation; therefore many of the same caveats cited above concerning why the comparison may not be fair still apply.

Finally, promising results have been obtained in a recent vortex simulation of Aarts and de Waele.[12] Using a different numerical simulation technique than Schwarz, they find, upon imposing a parabolic cross-channel $\mathbf{v}_n$ profile, that the line density is modified significantly as the vortex lines respond in a surprising way to the inhomogeneous velocity field.

II. APPARATUS

This experiment follows a standard thermal counterflow design. A schematic overview of the experimental apparatus is presented in Fig. 1. The flow channel connects a large helium reservoir to a small chamber containing a noninductively wound resistance heater. Intro-

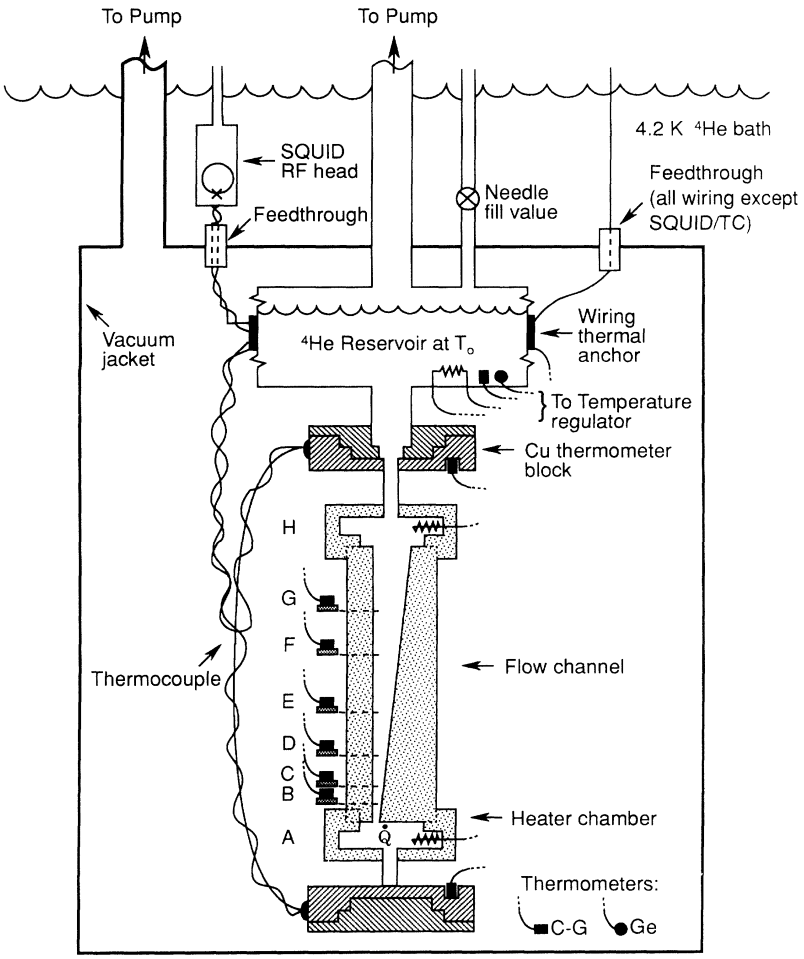

FIG. 1. Overview of apparatus. The flow channel and heater chamber are attached to the helium reservoir held at T_0, and isolated from the surrounding 4.2 K helium bath by a vacuum space. The thermocouple is shown connected across the entire channel, between r_A (heated end) and r_H (reservoir end), but either side can be moved to be connected instead to any other intermediate location, labeled B–G.

ducing power to the heater establishes a heat current $\dot{Q}$ in the channel. A regulator circuit controlled by an ac resistance bridge and lock-in amplifier holds the reservoir at a constant temperature $T_0 \pm 20$ μK. A vacuum jacket thermally isolates the reservoir, flow channel, and chamber from the surrounding 4.2 K helium bath. The thermal conductivity of the channel material and all electrical leads is small enough to ensure that the helium in the channel provides the only significant thermal path between the heated chamber and the reservoir.

The flow channel is depicted schematically in Fig. 2. Stycast 1266 epoxy is machined and assembled to form a 10 cm long rectangular channel of constant height $h = 0.025$ cm, but varying width. The width increases linearly with distance along the channel length from 0.2 cm at the narrow end to 1.0 cm at the wide end. This expansion of the aspect ratio from 8:1 to 40:1 represents a constant opening angle of $\theta = 0.08$ rad. Expressing the location along the channel length as a radial position r in cylindrical coordinates, the width at r is given by $w = \theta r$. Counterflow in this geometry therefore emulates a radially diverging heat flow originating from a source at $r = 0$, entering the channel at $r = 2.5$ cm and exiting at $r = 12.5$ cm. The laminar or turbulent dissipation associated with this counterflow establishes a temperature gradient throughout the channel, and so the temperature of the fluid at position r is raised above that of the regulated reservoir by an amount $\Delta T(r) = T(r) - T_0$. Although the present experiment studies diverging flow, the apparatus is designed so that the flow channel could be easily inverted to study converging flow. Another heater chamber is therefore located at the wide end of the flow channel, identical to the one at the narrow end, but unused in the present experiment. Each heater chamber, made of Stycast, is connected to a copper thermometer block. Depending on whether it is to serve as the reservoir or heated end, respectively, the thermometer block is then either attached to the large helium reservoir or blanked off via a copper flange, using an indium o-ring seal.

The temperature difference ΔT is measured with a Au-Fe thermocouple. The current produced in the thermocouple circuit is detected by a rf superconducting quantum interference device (SQUID) used as an ammeter, so that the voltage ΔV output by the SQUID is linearly proportional to ΔT. This technique has recently gained favor over standard resistance thermometry[13–15] for situations requiring a very sensitive differential measurement of temperature. In our experiment, the regulation fluctuations are sometimes larger than the smallest temperature differences $\Delta T(r)$ to be measured; however, because the regulation fluctuations cause the tempera-

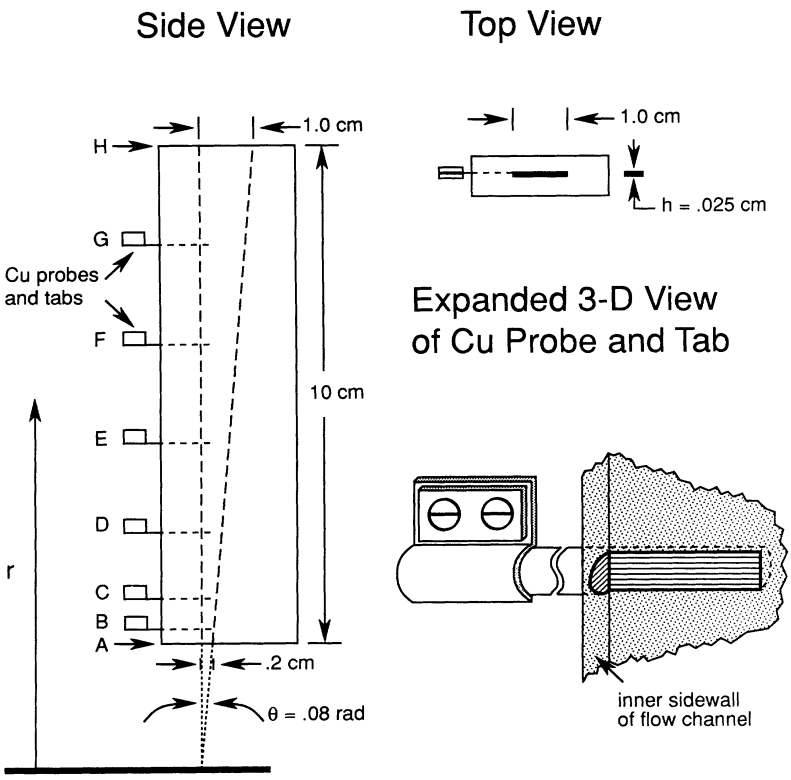

FIG. 2. Detail of the flow channel. The expanded view of probe and tab (drawn to approximate scale) shows how the copper wire has been cut away during the machining step that forms two adjacent walls of the flow channel, such that the exposed copper surface lies flush with these walls.

ture at every point in the channel to change simultaneously by the same amount, a measurement of the temperature *difference* between two positions in the channel is impervious to this overall variation in the absolute temperature. Following an innovation reported by Yamaguchi *et al.*,[16] we filled the shielding tubes housing the thermocouple wire and leads with Apezion-N grease to prevent the wires from vibrating, since motion of the wires in any magnetic field present induces rf noise. With this thermocouple-SQUID system, we can resolve a minimum temperature difference ΔT of 1 μK from background fluctuations, and measure voltage signals corresponding to temperature differences larger than 1 mK to within a $\pm 0.1\%$ accuracy.

To determine the temperature profile $T(r)$, the thermocouple can be connected between any two of eight locations along the channel length, including the heated chamber and reservoir at the respective ends of the channel. Probes made of copper wire embedded in the channel walls allow the temperature to be measured at six additional radial positions. These probes are distributed unevenly in position r, being concentrated near the narrow end of the channel where $\nabla T(r)$ was expected to be greatest. The probes are machined flush with the channel walls so that the exposed copper surface comes in direct contact with the helium, but does not protrude into the flow. A small copper tab soldered to the end of each wire outside the channel allows the thermocouple and/or a resistance thermometer to be attached (see Fig. 2).

Germanium or carbon glass resistors are used for regulation, for monitoring the temperature of the helium at various locations, and for calibrating the SQUID output. These resistors are first calibrated at each operating temperature T_0 against the 1958 ^{4}He temperature scale, the helium vapor pressure being measured with an MKS Baratron system. The usual procedure is to find the best linear fit to the resistance readings as a function of temperature, the slope dR/dT serving as a multiplicative constant to convert the measured change in resistance into the corresponding change in temperature. Because of the very large temperature differences generated across the channel in this experiment, a nonlinear fit to $R(T)$ had to be used here. The resistance calibration data for each T_0 was plotted "inverted" as T versus R, and the best third- or fourth-order polynomial fit to was found to $T(R)$ rather than to $R(T)$. The coefficients of this inverted fit are then easily used to convert a measured change in resistance into the corresponding change in temperature.

The resistors at the two radial positions spanned by the thermocouple provide a direct measurement of ΔT corresponding to the voltage reading ΔV output by the SQUID. The SQUID output is thus calibrated by simultaneously measuring ΔV and ΔT for various values of $\dot{Q}$. Only large values of $\dot{Q}$ can be used, since the resistors cannot resolve small values of ΔT with sufficient accuracy. Each measurement of ΔT is divided by the corresponding ΔV, and the best average value of this ratio is found. This voltage conversion factor decreases monotonically with temperature from 0.59 ± 0.02 mK/V at 1.3 K, to 0.51 ± 0.01 mK/V at 1.7 K, where the uncertainty has been estimated generously to encompass slight discrepancies measured among the various cooldowns and the somewhat large scatter found about the average value.

The uncertainty in this voltage conversion factor, which constitutes an overall systematic error of 2–3.5 % depending on the reservoir temperature, provides by far the largest single source of error in ΔT. We shall refer to this systematic error as the absolute error in ΔT.

In comparing the various data sets for a given reservoir temperature, the relative measurement uncertainty is much smaller, being limited by the SQUID sensitivity in measuring ΔV. Due to rf interference and thermal noise, the SQUID voltage signal fluctuates by ± 1–2 mV about a steady value (corresponding to underlying noise fluctuations in the thermocouple current of less than ± 0.1 nA). Our SQUID-thermocouple system can therefore measure a small ΔT signal to a relative accuracy of ± 1 μK. A different criterion determines the uncertainty in the SQUID measurement for larger temperature differences ($\Delta T > 1$ mK). The SQUID voltage signal ΔV rides on top of a base voltage level. This base line shifts up or down at random intervals by multiples of a characteristic step voltage (2.124 ± 0.001 V for our SQUID). These jumps occur because the SQUID temporarily "unlocks" and resets whenever it has exceeded its maximum output voltage of 10 V, and also when the ambient rf interference becomes too great. The measurement ΔV must be extracted from the actual voltage reading by adding or subtracting the appropriate number of voltage steps, producing an uncertainty in ΔV of $\pm 0.04\%$. The actual relative uncertainty for a large ΔT signal is taken to be somewhat larger, $\pm 0.1\%$, to account for a slight, slow drift in the base line voltage which sometimes occurs, another subtle effect of rf noise.

Two limits determined the maximum feasible heat current at each T_0. To ensure that the heat flux remained well below the value sufficient to initiate film boiling at the heater surface due to Kapitza resistance, we restricted our data collection to heat currents below $\dot{Q} = 10$ mW. We also did not extend our measurements beyond heat currents for which the temperature of the heated chamber exceeded that of the reservoir by more than about 50 mK, for three reasons. First, calibrating the resistors and accurately converting the resistance readings into temperature becomes increasingly difficult as the temperature range over which the calibration must be valid widens. Second, extracting ΔV from the voltage reading output by the SQUID becomes more painstaking due to the unlocking discussed above. Finally, any comparison of the data to theory becomes much more complicated if the temperature from one location in the fluid to another varies enough that the thermodynamic parameters describing the helium can no longer be treated as having constant values throughout the fluid. Within the temperature range studied, an increase in temperature of 10–20 mK is sufficient to alter the predicted behavior by 10%. Extending our measurements beyond $\Delta T = 50$ mK seemed pointless in light of the ensuing computational difficulty in performing an accurate theoretical calculation. Since no interesting new features were discovered in the data at the highest heat currents used, we were not compelled to relax these two self-imposed and somewhat arbitrary limits on the range of heat currents studied. Further details concerning the experimental apparatus and data collection method can be found in Refs. 17 and 18.

III. RESULTS

A. Notation

This experiment involved measuring the absolute temperature at, and temperature differences between, several locations in our diverging channel. Because keeping track of the various temperature measurements and many positions involved can become somewhat confusing, a careful definition of the notation used to refer to our measurements is in order before beginning a general discussion of our results. The thermocouple can be connected between any two of eight locations along the channel length. These radial positions are labeled alphabetically A–H in Figs. 1 and 2. The absolute temperature at a radial position r_i is denoted $T(r_i)$, whereas the temperature *difference* between two locations r_i and r_j is denoted $\Delta T(r_i, r_j) = T(r_i) - T(r_j)$, where $i, j \in (A, H)$. The wide end of the channel, located at r_H, is connected to the large reservoir held at temperature T_0; so $T(r_H) = T_0$. The increase in temperature at a particular position r_i over that of the reservoir is the quantity of primary interest, and so we shorten the notation $\Delta T(r_i, r_H)$ to simply $\Delta T(r_i)$, with the caution that one must clearly distinguish between $T(r_i)$ and $\Delta T(r_i) = T(r_i) - T_0$.

B. General features

The local temperature gradient is a function of both the position in the channel and the heat current $\dot{Q}$. We sought to map out these two dependences and understand the interplay between them. We proceeded by measuring the temperature difference over a fixed range in r, while varying $\dot{Q}$, then moving the thermocouple to span a new range in r and repeating the measurement in $\dot{Q}$. Because the thermocouple connection can only be moved by warming up the apparatus, the data for this experiment were taken in four series, each series corresponding to a different thermocouple positioning. Initially, the thermocouple was connected between the heated chamber at the narrow end of the channel at $r_A = 2.5$ cm and the reservoir at $r_H = 12.5$ cm to measure the temperature difference $\Delta T(r_A)$ across the entire flow channel. This series of measurements was conducted at five reservoir temperatures, $T_0 = 1.3$, 1.4, 1.5, 1.6, and 1.7 K. The data for $T_0 = 1.5$ K are shown in Fig. 3 and are representative of data at other reservoir temperatures. Measuring ΔT over other ranges in r yielded data with qualitatively the same features as are shown here for $\Delta T(r_A)$. These data all reveal a laminar flow regime for sufficiently small $\dot{Q}$, where the laminar temperature difference

$$\Delta T = \Delta T_L \tag{3}$$

depends linearly on $\dot{Q}$. Above a certain critical value of the heat current $\dot{Q}_c$ the system undergoes a discontinuous

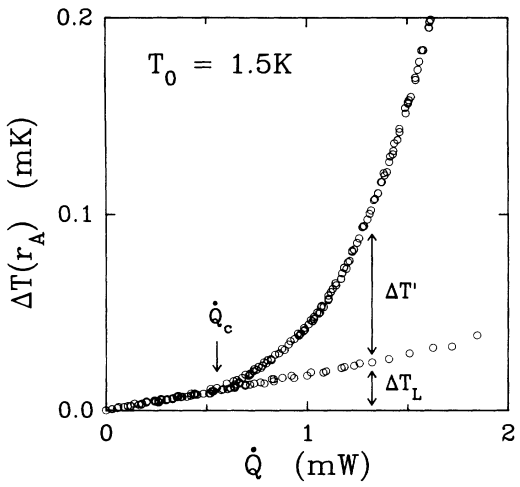

FIG. 3. Total temperature difference across the entire channel, $\Delta T(r_A)$, as a function of heat current for a typical data set, $T_0 = 1.5$ K. Only data for $\dot{Q} < 2$ mW are shown here to emphasize features. The full data set extends to $\Delta T \simeq 58$ mK at $\dot{Q} = 10$ mW. The laminar flow regime (ΔT linear in $\dot{Q}$) is clearly distinguishable from the turbulent regime (roughly cubic in $\dot{Q}$). For heat currents beyond $\dot{Q}_c$, the laminar state is metastable.

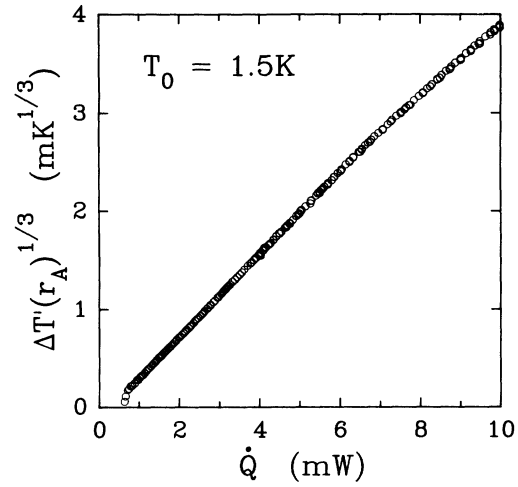

FIG. 4. Linearized plot of same data shown in Fig. 3. ΔT_L has been subtracted to yield the turbulent temperature difference $\Delta T'$. The cube root of $\Delta T'$ is plotted here to reveal the basic cubic dependence of $\Delta T'$ on $\dot{Q}$.

transition to a turbulent state characterized by a much larger temperature difference with an essentially cubic dependence on $\dot{Q}$. This transition is hysteretic, as can be seen in Fig. 3. The turbulent temperature difference $\Delta T'$ is taken to be the excess dissipation beyond the laminar value; so the total temperature difference is now

$$\Delta T = \Delta T_L + \Delta T' \ . \tag{4}$$

That this division of the measured temperature difference into a laminar and a turbulent piece is appropriate once the system is in the turbulent state is an assumption, but one well grounded in convention and supported by experimental evidence.[2] We therefore subtract ΔT_L from our measured signal to obtain $\Delta T'$. For values of $\dot{Q}$ much greater than $\dot{Q}_c$, the linear laminar piece is so insignificantly small in comparison to $\Delta T'$ that whether or not ΔT_L has been subtracted becomes immaterial. The general appearance of the turbulent state is qualitatively similar enough to that observed for a *uniform* high-aspect-ratio rectangular channel[19] to give one the initial impression that the homogeneous T-II state observed in uniform flows remains largely unaltered by the weak divergence imposed in this flow.

The same data displayed in Fig. 3 are graphed in a more informative manner in Fig. 4. To reveal the basic cubic dependence of $\Delta T'$ on $\dot{Q}$, the data have here been plotted as $(\Delta T')^{1/3}$ versus $\dot{Q}$. Linearizing the data in this manner immediately reveals two general features. First, the line formed does not extrapolate to intersect the origin, but rather is slightly offset, indicating that $\Delta T' \propto (\dot{Q}-\dot{Q}_0)^3$ would be a more appropriate functional form to describe the data. Second, rather than forming a perfectly straight line, the data exhibit a slight downward curvature at large $\dot{Q}$, appearing to indicate that the power-law dependence is not exactly cubic. This curvature can largely be attributed to the temperature dependence of the thermodynamic parameters characterizing the turbulent He-II, and would be present even if the power-law dependence on $\dot{Q}$ proved to be exactly cubic.

For the second data series, one end of the thermocouple was moved from the reservoir end, $r_H = 12.5$ cm, to an intermediate position in the channel, $r_D = 4.725$ cm. The other end was left attached to the heated end at $r_A = 2.5$ cm; the SQUID-thermocouple system then measured the temperature difference $\Delta T(r_A, r_D)$. To extract $\Delta T(r_D)$ from the measured quantity, since

$$\Delta T(r_A) = \Delta T(r_A, r_D) + \Delta T(r_D) \ , \tag{5}$$

a polynomial fit was first obtained to the corresponding data set of the previous series, $\Delta T(r_A)$ as a function of $\dot{Q}$, allowing interpolation of $\Delta T(r_A)$ at the values of $\dot{Q}$ for which $\Delta T(r_A, r_D)$ was measured; then the latter data set was subtracted from the fit to the former to yield $\Delta T(r_D)$. It would have been more straightforward to measure $\Delta T(r_D)$ directly, but without knowing *a priori* just how large $\Delta T(r_D)$ would prove to be, we opted for observing the complementary range in r to ensure that we would have a detectable signal, even at small $\dot{Q}$ and high T_0. Under the local uniformity approximation, $\Delta T(r_A, r_D)$ is predicted to be about 75% of the total temperature difference $\Delta T(r_A)$. Measurements of $\Delta T(r_A, r_D)$ were taken at the same five reservoir temperatures as before.

The third data series again involved moving only one end of the thermocouple, this time the one attached at r_A, to the new position $r_C = 3.47$ cm; so for this series $\Delta T(r_C, r_D)$ was measured, from which the temperature difference $\Delta T(r_C)$ was extracted. We were interested in examining a region of the flow far enough removed from the entrance and exit of the channel to avoid the influence of any possible end effects. In this data series, measurements were taken at only three reservoir temperatures

T_0 = 1.4, 1.5, and 1.6 K. For the last data series the thermocouple spanned the smallest region possible within the entrance of the channel, from r_A to r_B = 2.87 cm. Unfortunately, the SQUID apparatus did not function correctly after this final cooldown, but direct measurements of the temperature at r_B were still obtained for T_0 = 1.5 K from a carbon-glass thermometer attached to this probe location. Temperature difference data were similarly gathered in these last two series by resistance thermometers placed at two additional locations in the channel, r_E = 6.5 cm and r_F = 8.5 cm. Measurements at r_E were taken at T_0 = 1.3 and 1.5 K and at r_F only at T_0 = 1.5 K. Resistance thermometers lack the sensitivity of the SQUID-thermocouple system to discern a small ΔT signal from background noise, in part because they measure the absolute temperature rather than temperature differences, and so the measurements at these last three positions are useful only at the larger heat currents; nevertheless, the added information was gathered simultaneously with the SQUID-thermocouple data and proved valuable in quickly building a more complete picture of the temperature profile throughout the channel.

Once the temperature difference as a function of $\dot{Q}$ has been mapped out over several different ranges in r for a given reservoir temperature, the data can be graphed in a manner that better reveals the dependence of $\Delta T'$ on position r. The temperature profile throughout the channel, $\Delta T'(r)$, is plotted as a function of r for a fixed value of $\dot{Q}$. Figure 5 shows this temperature profile at T_0 = 1.5 K for a representative value of the heat current, $\dot{Q}$ = 5 mW.

C. Laminar flow

One should be able to predict the laminar dissipation $\Delta T_L(r)$ exactly by applying classical hydrodynamics in the two-fluid model to the specific geometry of the flow. Agreement of this theoretical prediction with the laminar data provides several essential checks on the experimental operation and design. First, if the functional forms of the predicted and measured laminar dissipation agree, then one may be confident that the flow channel has the shape expected and is not obstructed. Comparing resistance thermometry readings among the different data series independently verifies that the flow channel is not obstructed, at least by frozen air, since the apparatus is warmed up to room temperature between series. Second, finding the value of the channel height h which makes the predicted ΔT_L best fit the observed value provides an experimental determination of this crucial channel dimension, which is difficult to measure exactly by other means. Last, and most important to our purposes, the laminar prediction tests the validity of making the local uniformity approximation, in essence providing a measure of the weakness with which the flow diverges.

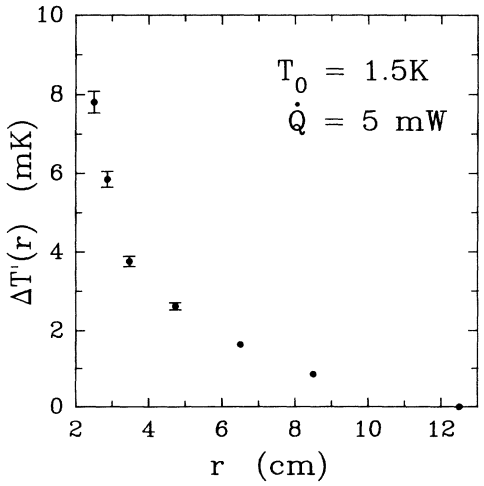

FIG. 5. Profile in r of the measured turbulent temperature difference $\Delta T'(r)$ at a typical heat current, $\dot{Q}$ = 5 mW. This profile graph combines the measurements at T_0 = 1.5 K from all data series. For example, only one point on this graph, that at r_A = 2.5 cm, is obtained from the data set depicted in Figs. 3 and 4. Error bars are shown when larger than the size of points.

Although the geometry of our flow channel does not readily lend itself to an analytic solution, an approximate solution is easily derived from the result for a *uniform* rectangular channel. An exact solution for the laminar temperature gradient in a uniform rectangular channel is obtained from the two-fluid equations of motion[20] and is given by

$$\nabla T_L = -\frac{12\,\eta\,\mathcal{F}}{\rho\,S\,h^2}\,V_n\,\hat{r}\ , \tag{6}$$

where the normal fluid flows in the direction $\hat{r}$ through the cross sectional area $A = h\,w$ of height h and width w [see Eq. (1)]. The negative sign indicates that ∇T_L increases in the direction opposite to $\mathbf{v}_n$. The aspect ratio $w : h$ of the channel determines the value of the geometric factor $\mathcal{F}$, which ranges from $\mathcal{F}$ = 2.371 for a square channel ($w:h = 1$) to $\mathcal{F} = 1$ for flow between two flat parallel plates ($w:h = \infty$).

For our diverging channel, where the width of the channel varies with position r as $w = \theta\,r$, we apply the local uniformity approximation by assuming that the local temperature gradient $\nabla T_L(r)$ at position r in our diverging flow is given by Eq. (6) upon replacing the constant value of V_n for uniform flow with the local value at position r,

$$V_n(r) = \frac{\dot{Q}}{\rho\,S\,T\,h\,\theta\,r}\ . \tag{7}$$

The local temperature gradient is then integrated over r to obtain the laminar temperature difference between any two positions in the channel. Other than V_n, the only factor in ∇T_L that varies with position is $\mathcal{F}$, which quantifies the influence of the channel sidewalls. At the narrow end of our channel, where $w:h = 8$, $\mathcal{F}$ = 1.086, and at the wide end, where $w : h = 40$, $\mathcal{F}$ = 1.016. Because the variation in $\mathcal{F}$ over the length of the channel is so small, $\mathcal{F}$ is treated as a constant to simplify the integration. Since ∇T_L is largest at small r, we use $\mathcal{F}$ = 1.086; therefore we may be slightly overestimating the actual predicted value of ΔT_L, but not by more than 7% at most. Integrating the uniform rectangle $\nabla T_L(r)$ in the

local uniformity approximation, we obtain the predicted laminar temperature difference between position r and the wide end of the channel at $r_H = 12.5$ cm:

$$\Delta T_L(r) = \frac{12\eta\mathcal{F}}{(\rho S)^2 T h^3 \theta}\dot{Q}\ln\left(\frac{r_H}{r}\right) . \quad (8)$$

This "integrated rectangle" solution does not account for the divergent nature of the flow, since the temperature gradient appropriate to a uniform, one-dimensional flow was used.

To determine whether the radial divergence alters the above prediction for ΔT_L substantially, we compared the above solution to two other approximate solutions, both of which incorporate the divergence explicitly but neglect the presence of the sidewalls. A solution for the laminar radial flow of an ordinary viscous fluid between two parallel disks has been presented by Savage[21] and expanded upon by Elkouh.[22] Our radially diverging flow represents an angular slice θ of the full 2π geometry treated by Elkouh. We generalized the Elkouh approach to the two-fluid model, making the minimal additional assumptions that the superfluid is incompressible, irrotational, and only has a component of velocity in the radial direction. The normal fluid velocity is assumed to have only radial and azimuthal components, and the solutions for $\mathbf{v}_n$ and ∇T_L are obtained via power series expansion. The other approximate solution for $\Delta T_L(r)$, which we term the "parabolic $\mathbf{v}_n$" solution, is obtained by invoking reasonable and minimal assumptions regarding the symmetries and properties of the flow in order to solve the two-fluid equations in closed form. First, it is assumed that the normal and superfluid components are incompressible ($\nabla\cdot\mathbf{v}_n = \nabla\cdot\mathbf{v}_s = 0$) and that $\mathbf{v}_n$ and $\mathbf{v}_s$ have only radial components. As before, $\mathbf{v}_s$ is assumed to be irrotational ($\nabla\times\mathbf{v}_s = 0$). To obtain an analytic solution for ∇T_L, the assumption that the cross-channel normal fluid velocity profile is parabolic is incorporated as an ansatz.

The Elkouh and the parabolic $\mathbf{v}_n$ solutions yielded nearly identical results, which agreed with the integrated rectangle solution for $\mathcal{F} = 1$, demonstrating the validity of using this simple expression [Eq. (8)] to compute ΔT_L in the local uniformity approximation. This integrated rectangle solution is compared to the data in Fig. 6, which shows the laminar thermal impedance $\Delta T_L(r)/\dot{Q}$ as a function of the reservoir temperature T_0. Of the four data series, only the first two measured ΔT over a large enough range in r to obtain accurate laminar data. The theoretical prediction is in excellent agreement with the data for $\Delta T_L(r_A)$ [see Fig. 6(a)]. For $\Delta T_L(r_D)$ the agreement is still very good, although, as seen in Fig. 6(b), the measured values are consistently about 20% larger than predicted. Since ΔT_L depends on the channel height as h^{-3}, a slight variation in this dimension, within the error limit of $h = 0.025 \pm 0.001$ cm, could partially account for this discrepancy. It was not possible to directly measure the channel height h, either optically or by any other nondestructive means, except at the channel ends. Another possible source of discrepancy not accounted for in the theoretical prediction of ΔT_L is that the normal fluid profile must develop over some entrance length, which could

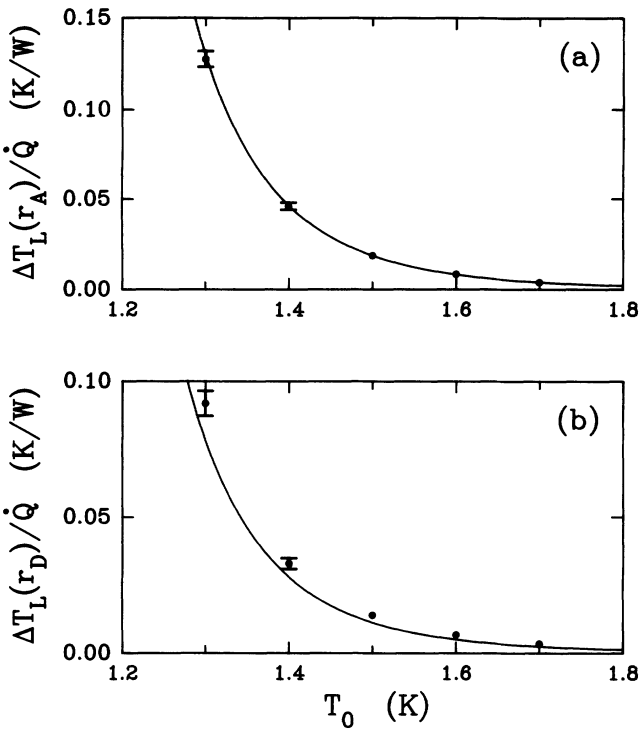

FIG. 6. Temperature dependence of the laminar thermal impedence $\Delta T_L(r)/\dot{Q}$ measured for (a) $r_A = 2.5$ cm and (b) $r_D = 4.725$ cm. Solid lines show the predictions of the "integrated rectangle" solution. The laminar temperature difference ΔT_L is linear in $\dot{Q}$, and so division by $\dot{Q}$ yields a constant thermal impedence at each reservoir temperature T_0. Error bars are shown when larger than the size of points.

alter $\Delta T_L(r)$ slightly; however, no evidence for a significant laminar entrance region has been observed, either in comparable experiments in uniform high-aspect-ratio rectangular channels[19] or in our results. We therefore believe laminar entrance effects, if any, to be unimportant. Overall, locally applying ∇T_L for a uniform rectangular flow satisfactorily predicts the observed laminar temperature profile in this diverging flow, providing convincing evidence that the divergence is indeed weak. It therefore seems reasonable to employ the same local uniformity approximation in modeling the turbulent state.

D. Schwarz model

Following the same prescription as for laminar flow, we apply the Schwarz model of homogeneous superfluid turbulence to this diverging flow by making the local uniformity approximation. The vortex line density is given in the Schwarz model as

$$L = \frac{{c_L}^2 V^2}{{\beta_S}^2} , \quad (9)$$

where

$$\beta_S = \frac{\kappa}{4\pi}\ln\left(\frac{1}{c_1 L^{1/2} a_0}\right) . \quad (10)$$

Here c_L and c_1 are temperature-dependent parameters predicted within the Schwarz model, κ is the quantum of circulation, and $a_0 \simeq 1.3 \times 10^{-8}$ cm is the effective core radius of a vortex line. The excess dissipation predicted by the Schwarz model,

$$\nabla T'(r) = -\frac{\kappa \alpha}{S}\left(I_{||} - c_L I_\ell\right) L V \hat{r} \ , \qquad (11)$$

is in excellent agreement with the T-II state observed in uniform flows. The friction constant α quantifies the frictional force the normal fluid exerts on the vortex lines, and $I_{||}$ and I_ℓ characterize the anisotropy of the vortex tangle; all are temperature-dependent parameters. We emphasize that the Schwarz parameters α, c_L, $I_{||}$, and I_ℓ are computed for a spatially homogeneous vortex tangle, and so any of these parameters may take on quite different values were the tangle spatially inhomogeneous. In the local uniformity approximation, L and $\nabla T'$ become spatial functions for our diverging flow, since the local average relative velocity $V = (\rho/\rho_s)V_n$, where V_n depends upon position [see Eq. (7)].

For a fixed value of the heat current $\dot{Q}$, the excess temperature difference $\Delta T'(r)$ is found by integrating Eq. (11) from r_H to r. This integration must be performed numerically since the integrand contains β_S, which depends logarithmically on r through L. A FORTRAN routine was written to iteratively compute β_S at each r for a fixed value of $\dot{Q}$, then integrate $\nabla T'(r)$ over r, and repeat the calculation for successive increments of $\dot{Q}$. The temperature dependence of all parameters in Eq. (11) was self-consistently taken into account throughout the integration.

Figure 7 compares the prediction of the local approximation to the measured temperature difference across the entire channel as a function of $\dot{Q}$ for each reservoir temperature T_0. Figure 7(c) contains the same data at $T_0 = 1.5$ K as were previously shown in Fig. 4. That the theory lines in Fig. 7 curve slightly downward at large $\dot{Q}$ is the result of the temperature dependence of the parameters and not a change in the functional dependence on $\dot{Q}$. Integrating $\nabla T'(r)$ *without* self-consistently updating all temperature-dependent parameters in the integrand to the local temperature (i.e., instead, leaving all temperature-dependent parameters "frozen" at the values appropriate to T_0) results in a slight upward curvature with increasing $\dot{Q}$ rather than the downward curvature seen here. This same downward curvature is evident in the data, but the magnitude of $\Delta T'(r_A)$ predicted by the theory is consistently larger than the data at all temperatures. Linearized graphs of $\Delta T'(r)$ versus $\dot{Q}$ at other positions r show similar systematic discrepancies between the observed and predicted values, with the data always extrapolating to a positive intercept in $\dot{Q}$. The Schwarz model applied locally cannot account for this nonzero $\dot{Q}$ intercept seen in the data.

The predictions of the local approximation are compared in Fig. 8 to the measured temperature profile $\Delta T'(r)$ at several values of the heat current for $T_0 = 1.5$ K. Figure 8(c) for $\dot{Q} = 5$ mW contains the same data as appeared in Fig. 5. Plotted in this way, the theoretical r dependence might not appear to be too dramatically different from that seen in the data, but the discrepancy between the two is actually quite large. The predicted r dependence in $\nabla T'$ is very close to r^{-3}, since $V \propto r^{-1}$ and $\nabla T' \propto V^3$. The only deviations from a purely r^{-3} dependence come from the logarithmic r dependence enfolded in β_S and the implicit r dependence introduced through the temperature variation of parameters. These latter two dependences add a gradual, smooth change in $\nabla T'$ with r to the basic r^{-3} dependence. Integrating $\nabla T'(r)$ therefore yields an r dependence of $\Delta T'(r)$ close to $(r^{-2} - r_H^{-2})$. This factor is divided out from both the data and the theory and the result displayed in Fig. 9. The dashed line is the result of a parametric fit to be discussed later. In Fig. 9, $\nabla T' \propto r^{-3}$ would appear as a straight horizontal line. We can deduce from Figs. 8 and 9 that that the turbulent temperature gradient does not depend on any single power of r throughout the channel. The data suggest that $\nabla T' \propto r^{-x}$ where at small r, $x \geq 3$ and at large r, $x \simeq 1$. The small deviation from a purely cubic r dependence inherent in the theory is manifestly different from the substantial and more complicated bimodal deviation exhibited in the data.

Clearly, the Schwarz model of homogeneous turbulence

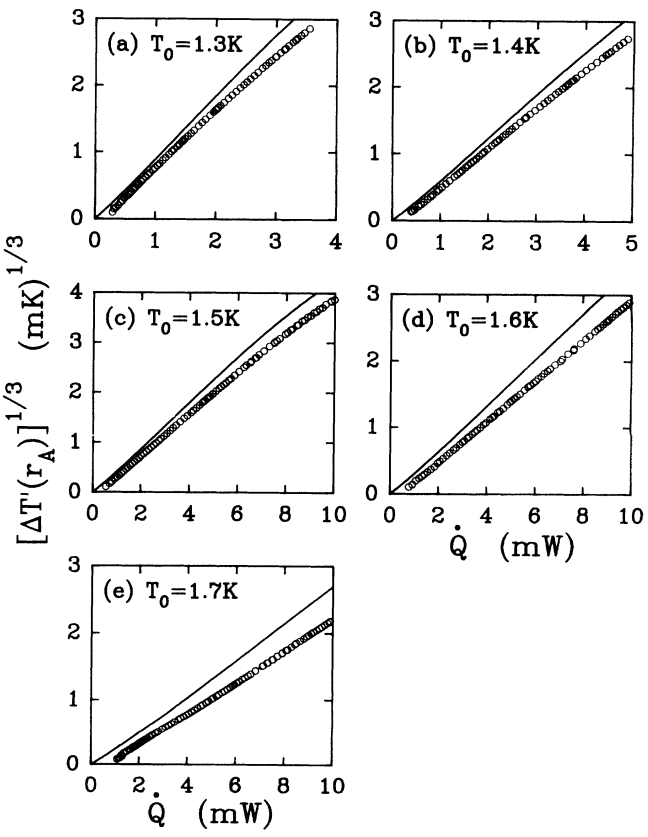

FIG. 7. Measured turbulent temperature difference $\Delta T'(r_A)$ (linearized by taking the cube root) as a function of heat current $\dot{Q}$ for all reservoir temperatures T_0 studied. The measurement uncertainty is much smaller than the size of points. Solid lines are the predictions of the homogeneous turbulence (Schwarz) model applied in the local uniformity approximation.

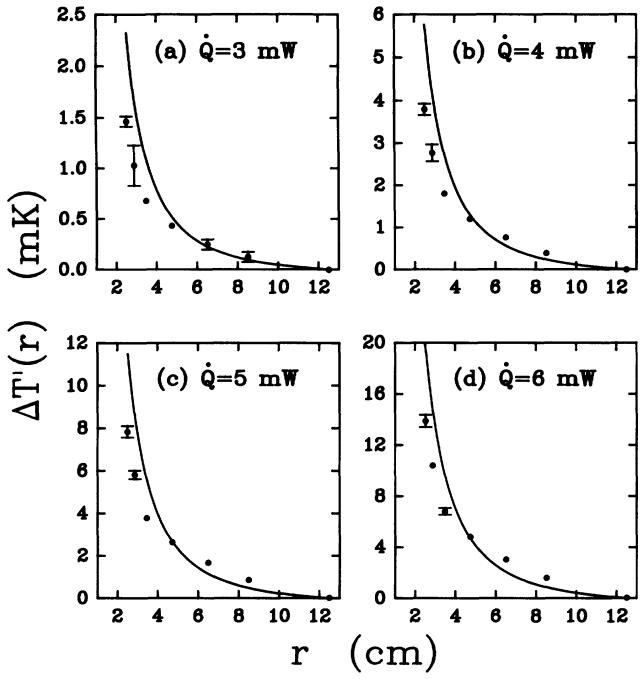

FIG. 8. Profile of the turbulent temperature difference $\Delta T'(r_A)$ as a function of r at $T_0 = 1.5$ K for four heat currents. Solid lines are the predictions of the Schwarz model of homogeneous turbulence applied locally. Error bars are shown when larger that the size of points.

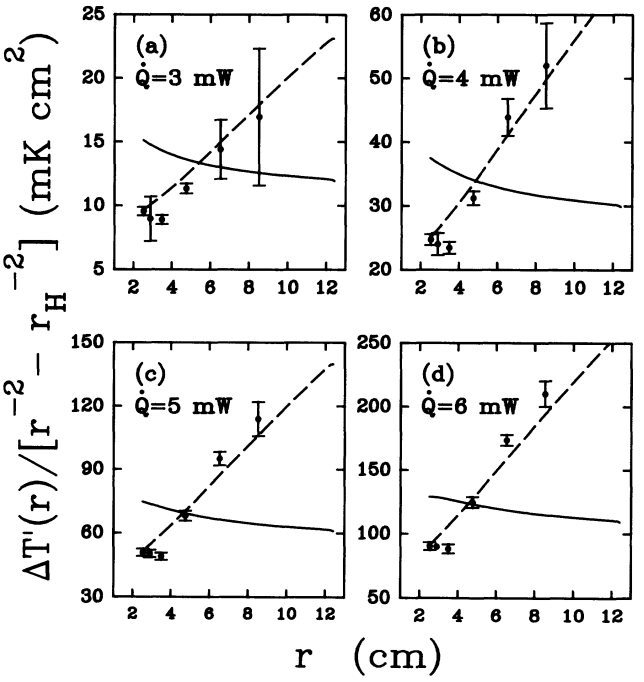

FIG. 9. Same data as shown in Fig. 8, here replotted with the major r dependence divided out. Predictions of the Schwarz model applied locally (solid lines, same as shown in Fig. 8) are contrasted with results of our modified line density fit (dashed lines) discussed in Sec. III F.

applied in the local uniformity approximation does not produce the correct functional dependence on either position r or heat current $\dot{Q}$ to agree with the data. In the Schwarz model the $\dot{Q}$ and r dependences enter together through $V \propto \dot{Q}/r$. Arbitrarily scaling the Schwarz parameters only changes the overall magnitude of $\nabla T'$, but does nothing to modify the $\dot{Q}$ or r dependence inherent in the homogeneous model. A correct theory of inhomogeneous turbulence must either modify the functional form of L itself, so that L is no longer proportional to V^2, or the relation $\nabla T' \propto L V$, or both. Whatever this modification might prove to be, it must serve to substantially alter the coupling between the $\dot{Q}$ and r dependences from that built into the homogeneous model.

We explored several *ad hoc* modifications to the Schwarz temperature gradient to see if some simple adjustment could better account for the observed temperature profile. A plausible first-order correction to the vortex line density was tested by adding a term proportional to ∇L to the expression for L given by Eq. (9) above. Modifying L in this way altered the r dependence of $\nabla T'(r)$, but in a direction opposite to that needed to agree with the data, and left the $\dot{Q}$ dependence unchanged.

E. Geurst hydrodynamic model

A new hydrodynamic model of turbulent superfluid helium, which purports to directly address the case of an inhomogeneous vortex line density, has recently been put forth by Geurst.[9] The Geurst model treats the vortex tangle as a third independent fluid, with velocity $\mathbf{v}_l$ equal to the drift velocity of the tangle and density L, on equal footing with the mass flow of the total fluid and the normal fluid component, with velocities $\mathbf{v}$ and $\mathbf{v}_n$ and densities ρ and ρ_n, respectively.[23] In contrast to other hydrodynamic models, such as proposed by Nemirovskii and Lebedev[24] or van Beelen, von Joolingen, and Yamada,[25] this three-fluid model explicitly accounts for the energy density and impulse (i.e., pseudomomentum) of the vortex tangle in the internal energy. By adding dissipative terms to the resulting equations of motion for the three fluids to account for the production of entropy and vortex line length, Geurst derives the equation of state for the vortex line density, arriving at a generalized form of the Vinen equation.

In the case of a large gradient in the vortex line density, such as might be present at a turbulent-to-laminar front, Geurst postulates adding a new term to the internal energy proportional to the gradient of the line density. This term strongly modifies the line density equation of state. Because this adjustment treats a spatial variation in the vortex line density, this model held the promise of addressing our experimental situation. At the time of our analysis, the Geurst model had only been presented for the simplest case of uniform flow in one dimension;[9,10] therefore, as we had done for the Schwarz model, we applied this one-dimensional (1D) model in the local uniformity approximation.

The 1D Geurst model contains six temperature-

dependent parameters which must be determined either by careful comparison to experiment or to a microscopic numerical simulation. Geurst provides the relation between five of these parameters and the analogous set of Schwarz parameters (c_L, α, α', $I_{||}$, and I_ℓ) in Ref. 10. The remaining parameter, called γ_ℓ, determines the strength of the new ∇L term added to the internal energy and therefore has no analog in the Schwarz model; so γ_ℓ must be treated as a free and tunable parameter.

Provided with this link to the Schwarz model, we attempted to apply the 1D Geurst model to our results. First, we generalized the 1D equations of motion to three dimensions (as much as possible) by substituting for all vector quantities the appropriate three dimensional analogs in cylindrical coordinates. We emphasize that this step alone falls far short of properly generalizing the Geurst model to three dimensions, since all the parameters involved, as well as their interpretation in the context of the Schwarz model, were determined for a one-dimensional, uniform flow. In fact, Geurst and van Beelen have recently provided a full three-dimensional (3D) version of this three-fluid model.[11] By contrast to the 1D version, the equations of motion in the full 3D model are much more complicated and contain no less than 23 independent parameters, which have yet be evaluated by comparison to an experiment or simulation. For the special case of homogeneous turbulence, the 3D Geurst model reduces to a slightly more general form of the 1D model, with the Vinen equation emerging in its familiar form, and the number of parameters collapsing to the above-mentioned five. The 3D version for the most general case of inhomogeneous turbulence in a nonuniform flow is daunting in its complexity, and not usable until the host of parameters it generates can be interpreted. The best we can do, therefore, is to employ the 1D Geurst model in the local uniformity approximation, cognizant of our underlying assumption, now embedded in many stages of the argument, that on a local level the turbulence bears the characteristics of a homogeneous tangle.

Our three-dimensional version of the 1D equation of state for the vortex line density in the presence of a large gradient in L is (see Ref. 9)

$$\frac{\partial L}{\partial t} + \nabla \cdot (L \mathbf{v}_l) + \kappa \frac{\gamma_\ell}{\gamma} \left[\frac{2}{L} (\nabla L)^2 - \nabla^2 L \right] = \frac{\beta}{2\gamma} L^{3/2} |\mathbf{v}_l - \mathbf{v}| - \frac{\beta_S}{\gamma} L^2 \ . \quad (12)$$

The Geurst parameters γ and β are related to the Schwarz parameters by

$$\frac{\beta}{2} = \left[\left(\alpha' I_{||} - \frac{\rho_n}{\rho} \right) \frac{1}{c_L} + (1 - \alpha') I_\ell \right]^{-1} , \quad (13a)$$

where

$$\frac{\beta}{2\gamma} = \alpha I_\ell \left(\alpha' I_{||} - \frac{\rho_s}{\rho} \right)^{-1} \quad (13b)$$

and α' is a second-order friction coefficient in the Schwarz model. It should be noted that in the case of a spatially homogeneous L, the Schwarz (or Vinen) expression for the vortex line density, Eq. (9), is recouped.

We seek the steady-state solution of Eq. (12) for the case of zero net mass flow ($\mathbf{v} = 0$). This highly nonlinear second-order differential equation can only be solved in some approximation which simplifies it. The simplification we explored was to neglect the second derivative term $\nabla^2 L$ in favor of the first derivative squared term $(\nabla L)^2/L$. In justifying this approximation, we first observe that if the line density varied as a simple power of r, $L = Cr^n$, then $(\nabla L)^2/L = \nabla^2 L = n^2 C r^{n-2}$. For such a simple line density, since these two terms would have the same functional dependence, each would introduce a variation that decouples the $\dot{Q}$ and r dependences in L in exactly the same way. The character of the line density which is an exact solution to Eq. (12), if it is to fit our data, must be such that these two terms still behave very analogously to one another and the above remarks would still largely hold true. Choosing which of these terms to retain and which to discard seems more a matter of computational convenience than a substantive issue, and so it seems reasonable to replace the difference of these two terms with a single term written either as $\nabla^2 L$ or $(\nabla L)^2/L$. Since the prefactor multiplying the expression in square brackets in Eq. (12) contains the adjustable parameter γ_ℓ, the choice of which one of these two terms is used becomes absorbed in the magnitude and algebraic sign of γ_ℓ; therefore the entire possible range of positive and negative γ_ℓ values was considered.

Choosing to drop the Laplacian term in favor of the $(\nabla L)^2$ term yields a quadratic equation in ∇L of the form

$$A(\nabla L)^2 + B \nabla L + C = 0 \ , \quad (14)$$

where the coefficients A, B, and C are functions of L and the Geurst parameters:

$$A = \frac{2\kappa\gamma_\ell}{L\gamma} \ , \quad (15a)$$

$$B = |\mathbf{v}_l| \ , \quad (15b)$$

$$C = \frac{\beta_S}{\gamma} L^2 - \frac{\beta}{2\gamma} L^{3/2} |\mathbf{v}_l| \ . \quad (15c)$$

In this approximation, Eq. (12) is reduced to a first-order equation that is relatively easy to solve. Being only first order, Eq. (14) requires only one boundary condition, the value of L at the entrance (or exit) of the channel, $L(r_A) = L_e$. Equation (14) only predicts the derivative of L at a given position r, not L itself. The two roots to this equation are referred to here as the "plus" and "minus" roots, corresponding to choosing the plus or minus sign, respectively, before the square root of the discriminant $(B^2 - 4AC)$. To solve for $L(r)$, one root of the equation is selected, and values of the two adjustable parameters L_e and γ_ℓ are chosen. Having thus fixed both L and ∇L at $r = r_A$ (or r_H), an iterative procedure is used to map out $L(r)$ throughout the channel for the particular combination of parameters and root specified.

Due to the highly nonlinear nature of Eq. (14) and the resulting strong dependence of both the sign and magnitude of $\nabla L(r)$ on $L(r)$ and γ_ℓ, we were compelled to explore the full range of parameter space for both roots. In addition, there remains some question as to whether

the vortex lines in fact drift in the same direction as, or opposite to, the normal fluid.[26] Reversing the direction of $\mathbf{v}_l$ reverses the algebraic sign on the divergence term $B\nabla L = \mathbf{v}_l \cdot \nabla L$. Experiments which have attempted to directly measure $\mathbf{v}_l$ have obtained somewhat ambiguous and conflicting results.[27] We therefore allowed the value of B in Eq. (14) to vary from $+\mathbf{v}_l$ to $-\mathbf{v}_l$ by introducing a third adjustable parameter $-1 < \phi < 1$ multiplying B. In all, we had eight possible classes of the solution to Eq. (14) to consider, corresponding to the eight combinations of choices of the root of the equation (plus or minus) and the algebraic signs of $\gamma_\ell(\pm)$ and $\phi(\pm)$. For each of these eight regions in parameter space, only limited ranges of the values of L_e, γ_ℓ, and ϕ lead to a viable solution for all r within $2.5 \leq r \leq 12.5$ cm.

Of the eight classes, four lead to unphysical solutions where L either decays immediately to zero, or diverges equally rapidly, from the starting L_e. Two more classes, for the case of $\phi < 0$ and starting from a small initial value L_e, yield a solution where L increases very gradually over some length δ within the channel entrance; then over a very small range in r about $r = r_A + \delta$, L grows explosively to a value $L \gg L_e$. With this increase in L, the relative importance of the terms in A and B in Eq. (14) diminishes in comparison to the role of C in determining the steady-state line density; so for $r > r + \delta$, $L(r)$ is nearly the same as is predicted in the Vinen or Schwarz model. This solution reproduces a result first obtained by Murphy, Tough, and Fiszdon, who added a term of the form $\nabla \cdot (L\,\mathbf{v}_l)$, with $\mathbf{v}_l < 0$, to the Vinen equation.[28] The line density obtained in that solution matched that given by the Schwarz (or Vinen) model of homogeneous turbulence in the local uniformity approximation everywhere in the channel except within a distance δ of the entrance, where L decreased rapidly until it had "accommodated" to the much lower value outside the channel. Upon completion of only the first two series of measurements, we had only the two data points at $r_A = 2.5$ cm and $r_D = 4.725$ cm in Fig. 8, from which it seemed that $\Delta T'(r_D)$ was correctly predicted by the Schwarz model, but $\Delta T'(r_A)$ was much smaller than expected. Our initial findings could be explained by supposing that a fairly large entrance region existed, on the order of $\delta = 0.5$ cm in size, over which the vortex line density was suppressed much below the value expected from the Schwarz model. After obtaining a more complete picture of the temperature profile $\Delta T'(r)$, however, it became obvious that no such pronounced entrance effect exists, and the apparent agreement between the Schwarz model and the data in the vicinity of r_D is serendipitous.

Only one class of the Geurst solution, corresponding to choosing the minus root to the quadratic and $\phi > 0$, $\gamma_\ell > 0$, produced a line density profile which had a suitable functional form and overall magnitude to potentially describe our data.[29] The resulting Geurst $L(r)$ was inserted into the Schwarz expression for $\nabla T'$, which was integrated to obtain $\Delta T'(r)$. The corresponding Geurst expression for $\nabla T'$ yielded nearly the same result for the range of parameter space in question, and so using the simpler Schwarz expression for $\nabla T'$ does not introduce any inconsistency. In seeking a fit to the data, the line density L_e at the channel entrance will of course increase with $\dot{Q}$, but γ_ℓ should depend on temperature only, and so the same value of γ_ℓ should provide a reasonable fit to the temperature profile $\Delta T'(r)$ at different $\dot{Q}$ values for a given T_0. No such overall fit to the data was found. At best, for a given $\dot{Q}$, a combination of L_e and γ_ℓ could be identified that yielded a reasonable fit to our temperature profile data at small r ($r < 3.5$ cm). This "close fit" proved untenable upon changing $\dot{Q}$ slightly while holding the value of γ_ℓ fixed, since no new value of L_e could be found to similarly fit our results over *any* range in r at the new $\dot{Q}$.

The calculation performed and assumptions adopted in applying the Geurst model were thoroughly checked for accuracy and sensibility. Inputting the line density at the channel exit as the boundary condition to iteratively map out $L(r)$ while decreasing r yielded the same result as did starting at the entrance and increasing r. As a final check on our assumptions, we estimated the size of the neglected $\nabla^2 L$ term in comparison to the $(\nabla L)^2/L$ term kept. For the "closest fit" obtained at a given $\dot{Q}$, $\nabla^2 L$ was of the same order of magnitude, but somewhat smaller than, $2(\nabla L)^2/L$. More important, these two terms exhibited nearly the same functional dependence on r. It is interesting to note that a comparable fit at small r to the "closest fit" achieved with the Geurst model can be obtained from the Schwarz model by decreasing c_L by 16%. (The dashed line in Fig. 10 depicts precisely this scaling of c_L.) Despite the promise of handling a nonuniform line density, the 1D Geurst model, when applied as we have here, at best yields a solution which does not differ much in functional form from that obtained using the Schwarz or Vinen model in the local uniformity approximation.

F. Modified line density

Since none of the existing theoretical models adequately describe our results, we present an empirical fit that succinctly summarizes our data. The following modification to the vortex line density captures the general features of our observations and constitutes a three-parameter fit to our data. By scaling the local homogeneous line density $L = L_h$ [Eq. (9)] and adding to it a polynomial in $\dot{Q}$, we obtain the modified line density

$$L = g_0 L_h + g_1 \dot{Q} + g_2 \dot{Q}^2 \,, \tag{16}$$

to be inserted in the Schwarz expression for $\nabla T'(r)$ given in Eq. (11). For each reservoir temperature, we were able to identify a unique set of parameters g_0, g_1, and g_2 that provide excellent agreement with our data. Although these parameters depend only on temperature, it is possible that enfolded in their values is some "hidden" dependence on the specific geometry of our experiment. By hidden we mean some factor which remains fixed throughout our experiment, such as the opening angle θ or the channel height h. Any forthcoming model of inhomogeneous turbulence, or any generalization or alteration of existing theory purporting to address nonuniform flows, ought to yield a line density in agreement

with the above form when applied to our flow geometry.

The addition of the polynomial function of $\dot{Q}$ to the line density adjusts both the $\dot{Q}$ and r dependences of $\nabla T'(r)$ appropriately. Since L is multiplied by V in forming $\nabla T'$, and $V = C\dot{Q}/r$, the functional form of $\nabla T'$ becomes

$$\nabla T' = -F(T)\left[g_0 C^2 \left(\frac{c_L}{\beta_S}\right)^2 \frac{\dot{Q}^3}{r^3} + g_1 \frac{\dot{Q}^2}{r} + g_2 \frac{\dot{Q}^3}{r}\right]\hat{r}\ , \tag{17}$$

where all other temperature and geometric dependences are contained in $F(T)$ and C. At sufficiently small r, this modified temperature gradient is dominated by the local homogeneous contribution, which varies as r^{-3}. For r less than $\sim$ 4 cm, the r dependence of L_h follows that of the data, but the Schwarz model results in a temperature difference that is always much too large in magnitude at small r (see Figs. 8 and 9). We therefore multiply L_h by g_0, where $0 < g_0 < 1$, to scale back the contribution of this local homogeneous piece. Adding the polynomial in $\dot{Q}$ to L_h introduces an r^{-1} dependence in $\nabla T'$ which allows the bimodal dependence on r observed in the temperature profile to be fit reasonably well throughout the channel. Upon integrating $\nabla T'$ from r_H to r, the resulting $\Delta T'(r)$ is now a polynomial in $\dot{Q}$ with a quadratic as well as cubic term. Together these two terms act as the two highest-order terms in the expansion of $(\dot{Q} - \dot{Q}_0)^3$. The added quadratic piece, $\Delta T' \propto g_1 \ln(r_H/r)\dot{Q}^2$, accounts for the nonzero $\dot{Q}$ intercept seen in Fig. 7, provided that $g_1 < 0$. The new cubic piece $\Delta T' \propto g_2 \ln(r_H/r)\dot{Q}^3$ combines with the local homogeneous piece, also cubic in $\dot{Q}^3$; therefore increasing g_2 increases the slope of $\Delta T'^{1/3}$ versus $\dot{Q}$.

The following procedure was used to obtain the values of g_0, g_1, and g_2 which best fit the data. First, we focused our attention on the linearized plot of $\Delta T'(r_A)^{1/3}$ versus $\dot{Q}$. Picking a value of g_0 in the range 0.25–0.75 and temporarily fixing the value of g_1, we tuned the value of g_2, selecting the value of g_2 that yielded the best match to the slope of the data for that g_0. Since g_1 controls the $\dot{Q}$ intercept of the curve, we then identified the value of g_1 needed for each combination (g_0, g_2) to fit the intercept as well as slope.

From this first data series, we therefore matched the "candidate pairs" of (g_0, g_2) values to their g_1 "running mates." A sample of the modified $\Delta T'(r)$ profile resulting from four such combinations of all three parameters is compared to the data for $\dot{Q} = 5$ mW at $T_0 = 1.5$ K in Fig. 10, curves (a)–(d). For comparison, the result of using the local homogeneous line density alone, scaled to fit $\Delta T'(r_A)$ for $\dot{Q} = 5$ mW, is displayed in curve (e). Although using the local homogeneous line density scaled by $g_0 = 0.70$ (setting $g_1 = g_2 = 0$) appears to fit the temperature profile data fairly well at small r, this fit bears the wrong $\dot{Q}$ dependence, and so it does not agree with the data at other $\dot{Q}$. Examining the four candidate trios for the modified line density, we see that the effect of adding the polynomial in $\dot{Q}$ to L_h is to increase $\Delta T'$ at large r. As g_2 is increased, g_0 must be correspondingly decreased to maintain the fit at r_A.

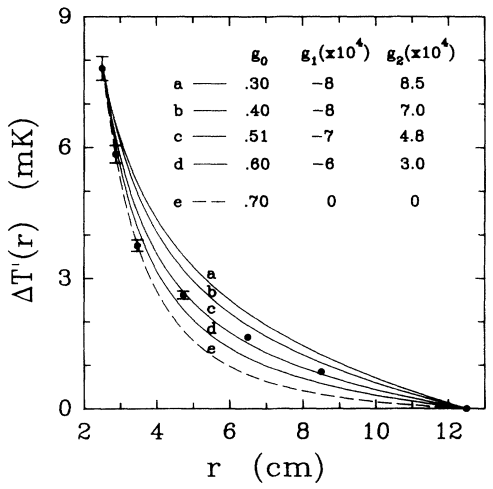

FIG. 10. Curves (a)–(d) (solid lines): Testing four candidate trios of fit parameters (g_0, g_1, g_2) for the modified line density formula at $T_0 = 1.5$ K. All four match the measured $\Delta T'$ equally well at $r_A = 2.5$ cm. Data and fits are shown here for $\dot{Q} = 5$ mW, but the same fit parameters in (a)–(d) agree equally well with $\Delta T'(r_A)$ over the *entire range* in $\dot{Q}$. Only curve (c) also fits the data at $r_D = 4.725$ cm for all $\dot{Q}$. Curve (e) (dashed line): Using only the homogeneous line density, scaled to fit the measured $\Delta T'(r_A)$. This fit agrees with the data at small r, but *only* for $\dot{Q} = 5$ mW.

To identify the best fit to the actual temperature profile, the particular trio (g_0, g_1, g_2), which also provides a good fit to the second data series, $\Delta T'(r_D)$ versus $\dot{Q}$, is selected. A quick glance at Fig. 10 suggests that the best combination is apparently that of curve (c), namely, $g_0 = 0.51$, $g_2 = 4.8 \times 10^4$ (mW cm)$^{-2}$, and $g_1 = -7 \times 10^4$ mW^{-1} cm^{-2}, but this graph is for a fixed heat current, $\dot{Q} = 5$ mW. That this trio of parameters indeed provides the best overall fit can better be seen by comparing the $\dot{Q}$ dependence of this fit to that of the observed temperature differences $\Delta T'(r_A)$ and $\Delta T'(r_D)$, as shown in the linearized graphs in Fig. 11. The parameters were chosen specifically to fit the slope and intercept of the first data series, and so the excellent agreement obtained in Fig. 11(a) is nothing more than what was demanded from the outset. In fact, all four candidate trios identified [curves (a)–(d) in Fig. 10] yield equally good fits to $\Delta T'(r_A)$ over the full 10 mW range in $\dot{Q}$. Only one of these, the combination of g_0, g_1, and g_2 discussed above and displayed in curve (c) of Fig. 10, also fit $\Delta T'(r_D)$ equally well over a wide range in $\dot{Q}$, as shown in Fig. 11(b). The same temperature profile data displayed in Fig. 10 are shown in Fig. 9(c), where the dominant r dependence has been divided out. In Fig. 9, the best-fit modified line density prediction (dashed lines) is compared to the Schwarz homogeneous model (solid lines) for several values of $\dot{Q}$. Although our empirical fit only matches the data closely at positions r_A and r_D, as demanded, it clearly tracks the both the $\dot{Q}$ and r dependences of the data much better than does the local homogeneous model.

The best-fit trio of parameters for each reservoir tem-

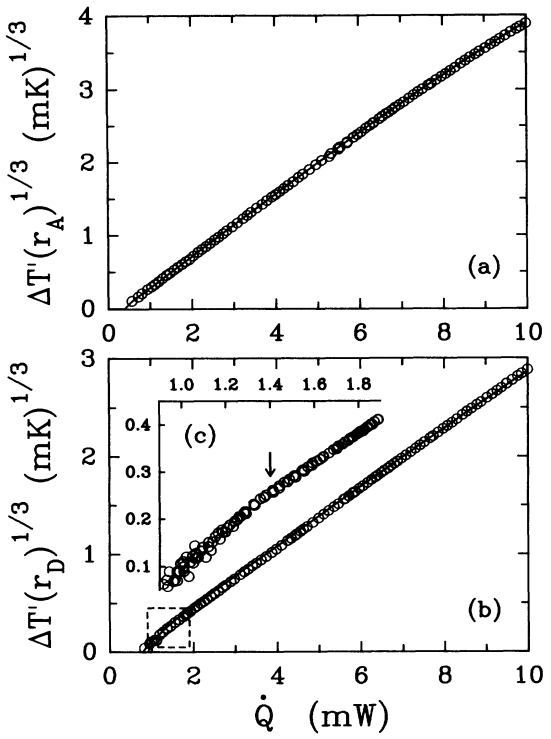

FIG. 11. Linearized $\Delta T'$ versus $\dot{Q}$ at $T_0 = 1.5$ K, shown for two positions in r: (a) $r_A = 2.5$ cm [same data as shown in Fig. 7(c)] and (b) $r_D = 4.725$. Solid lines are the predictions of the modified line density formula, using the best-fit set of parameters (g_0, g_1, g_2) [listed in Table I and also shown in Fig. 10(c)]. Inset (c) shows an expanded view of the data in the boxed region in (b). The arrow marks the change in slope caused by the turbulent-laminar front exiting the channel.

perature is listed in Table I. This parametric fit works as well at the other reservoir temperatures as has been illustrated here for $T_0 = 1.5$ K. Our measurements at any T_0 can therefore be quickly and easily reconstructed with reasonable accuracy by inserting the appropriate trio of parameters from Table I into the modified line density formula [Eq. (16)]. The measurements of $\Delta T'(r_A)$ and $\Delta T'(r_D)$ can be rendered with great precision, and the temperature differences at other positions r approximated with only small systematic variations from the actual measured values, provided that the same procedures as we used are followed in the computations, as several subtleties of the modified line density calculation

TABLE I. Best-fit values of parameters g_0, g_1, and g_2 at each reservoir temperature.

T_0 (K)	g_0 --	g_1 ($\mathrm{mW^{-1}\,cm^{-2}}$)	g_2 ($\mathrm{mW^{-2}\,cm^{-2}}$)
1.3	0.50 ± 0.02	$(-8.0 \pm 2.0) \times 10^4$	$(1.4 \pm 0.1) \times 10^5$
1.4	0.49 ± 0.01	$(-7.0 \pm 1.0) \times 10^4$	$(8.6 \pm 0.2) \times 10^4$
1.5	0.51 ± 0.01	$(-7.0 \pm 0.5) \times 10^4$	$(4.8 \pm 0.2) \times 10^4$
1.6	0.47 ± 0.01	$(-6.0 \pm 0.5) \times 10^4$	$(2.6 \pm 0.1) \times 10^4$
1.7	0.39 ± 0.01	$(-4.0 \pm 0.5) \times 10^4$	$(1.5 \pm 0.1) \times 10^4$

are important to the outcome. Anyone employing the contents of Table I to recoup our results should consult Ref. 18 for further details regarding these procedures.

As a check on our methodology, we instead used the uniform local line density $L = L_h$ and corresponding β_S and modified $\nabla T'$ directly, by scaling the homogeneous temperature gradient (resulting from L_h) by g_0 and adding to it the same polynomial in $\dot{Q}$ as before, to once again obtain Eq. (17) for $\nabla T'$. This latter approach therefore modifies the expression for $\nabla T'$ in the same manner as before, but does not introduce the modification through L itself. The only distinction in practice between these two approaches lies in the values of β_S computed and inserted in Eq. (17). An equally good fit to the data can still be achieved, but with different values of g_0, g_1, and g_2 than are listed in Table I. Whether the modification to the local uniformity approximation is introduced in the line density or only in the temperature gradient is immaterial inasmuch as either way this method is no more than a parametric fit to the data, but it seems more sensible to modify the line density from the local homogeneous expression than to alter the basic relation $\nabla T' \propto LV$.

Although we hesitate to assign physical significance to the form of the modified line density, it is interesting to note that since the polynomial $g_1\dot{Q} + g_2\dot{Q}^2$ contains no r dependence, this piece of the modified line density is a constant everywhere in the channel for any given $\dot{Q}$. It is as if the local homogeneous line density, which is determined by the local velocity, is superimposed on top of a constant or average background line density. In fact, spatially averaging the local homogeneous part of the line density $g_0 L_h$ over the channel volume yields a result about equal, at each $\dot{Q}$, to this added constant piece. It is worth pointing out that in the case of a uniform flow the local homogeneous line density is itself constant throughout the channel, and therefore would be indistinguishable from a constant background line density. In our modified line density formula, L_h was scaled by g_0. It would be entirely consistent with the data for uniform flows to similarly rescale the local homogeneous line density, and then add to it a spatially averaged contribution to make the total line density once again equal to the original L_h predicted by the Schwarz model. Although it would be presumptuous to push this speculation too far, the fact that in a uniform flow one cannot distinguish between a vortex line density governed solely by the local velocity field and a line density representing some sort of spatially averaged background level bears some consideration.

G. A Stationary turbulent front

Our measurements of the temperature profile along the channel length give us insight into one final question: How does the onset regime for superfluid turbulence in a nonuniform flow compare to that in a uniform flow? At heat currents just above the minimum needed to sustain turbulence, we observe the formation of a stable and stationary turbulent-laminar front within our diverging channel. At such moderate values of $\dot{Q}$, we measure a to-

tal temperature difference in excess of the laminar value at small r, whereas at larger r, $\Delta T(r) = \Delta T_L(r)$, indicating that at some intermediate position in the channel the flow undergoes a transition from a turbulent to the laminar state. Not unexpectedly, at the minimum $\dot{Q}$ for which the turbulent state persists, only a small region of the flow near the narrow end of the channel — where the local velocity is largest — is turbulent. As the heat current is increased, the turbulent-laminar front moves out to larger r, until eventually the front reaches the wide end and the entire channel is filled with turbulence.

We identify the critical value of the heat current at which the front reaches each probe location r by graphing $\Delta T(r)$ versus $\dot{Q}$ for each position probed. For example, as shown in Fig. 3, at the channel entrance $\dot{Q}_c = 0.55 \pm 0.05$ mW for $T_0 = 1.5$ K. Figure 12 displays the critical heat current $\dot{Q}_c$ as a function of r for $T_0 = 1.5$ K. The measurements at $r = 6.5$ and 8.5 cm were made with resistance thermometers, which are far less sensitive than the SQUID-thermocouple apparatus; therefore, only an upper bound for $\dot{Q}_c$ could be determined from these data sets. As a logical lower bound, $\dot{Q}_c$ must be larger at these locations than the value observed at smaller r.

Rather than being directly measured as for the other positions, the point in Fig. 12 at the wide end of the channel, $r_H = 12.5$ cm, is inferred from the linearized graph of $\Delta T'(r_D)$ versus $\dot{Q}$, which exhibits a subtle but distinct change in slope in the region around $\dot{Q} = 1.4$ mW, as shown in the inset (c) in Fig. 11. For $\dot{Q} < 1.4$ mW, the slope is steeper than at large $\dot{Q}$, and $\Delta T'$ is smaller than would be estimated from an extrapolation of the high-$\dot{Q}$ behavior. This change in slope presumably occurs at the heat current at which the turbulent-laminar front is located at the wide end of the channel. Below $\dot{Q} = 1.4$ mW, part of the channel is still in the laminar

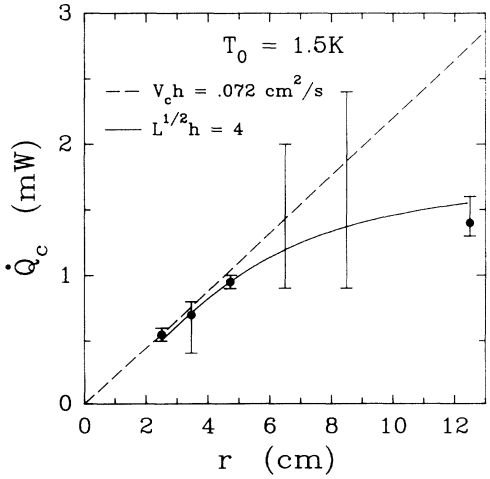

FIG. 12. Critical heat current as a function of r, indicating the formation of a stable, stationary turbulent-laminar front. Points with error bars are obtained from the SQUID-thermocouple measurements; resistance thermometers yield only upper and lower bounds for $\dot{Q}_c$ (no points). Solid line: curve of constant line density. Dashed line: curve of constant critical velocity.

state and $\Delta T'$ is correspondingly smaller than if the entire flow were turbulent. Above $\dot{Q} = 1.4$ mW, the entire channel is in the turbulent state.

To test our interpretation of this change in slope, we simulated the presence of a turbulent-laminar front using the modified line density model described in the previous section. Although the exact critical condition causing the turbulent state to collapse is not known, a simple assumption is that turbulence cannot be maintained once the average relative velocity V falls below some minimum critical value V_c. Adopting this criterion, we adjusted our model to arbitrarily set $L = 0$ for all positions r for which V was less than a chosen value V_c. The modified line density model, supplemented in this manner by a front, yields a cusp in the slope of $\Delta T'^{1/3}$ versus $\dot{Q}$ at precisely the value of $\dot{Q}$ corresponding to the velocity at wide end of the channel being at V_c. Without a front, the model predicts a uniform slope over the whole range in $\dot{Q}$. Rather than a critical velocity, the condition determining where the turbulent-laminar transition occurs could be a minimum line density below which turbulence cannot be maintained. This criterion was also easily modeled using our modified line density formula, resulting again in an abrupt change in slope in the linearized $\Delta T'$ graph similar to that generated by assuming a critical velocity.

For a reasonable value of V_c, this shift in slope is discernable in the modeled behavior of $\Delta T'(r)^{1/3}$ versus $\dot{Q}$ for any position r, but for small r becomes a very subtle effect, too small to resolve in the data. That we do not observe a change in slope in the linearized graphs of $\Delta T'(r_A)$ or $\Delta T'(r_A, r_D)$ versus $\dot{Q}$ is explained by the highly nonlinear nature of the turbulent temperature gradient. The overwhelming contribution to the temperature difference across the entire channel is coming from the large $\nabla T'$ at the narrow end. Whether the flow farther down the channel is laminar or turbulent makes little difference since $\Delta T'(r_A)$ is so dominated by the action at the narrow end. For a range in position near the wide end of the channel, the laminar region beyond the front plays a larger relative role in reducing $\Delta T'$ and a more noticeable change in slope results. We could only distinguish the cusp in graphs of $\Delta T'(r_D)$. Since this data set is obtained by subtracting measurements of $\Delta T(r_A, r_D)$ from a fit to $\Delta T(r_A)$, generous error bars are assigned to the exact location of the cusp, and hence to $\dot{Q}_c$ at $r_H = 12.5$ cm. Careful error analysis confirms that the change in slope is a real, albeit subtle, feature of the data and not some numerical artifact of the process used to extract $\Delta T'(r_D)$ from the directly measured quantities.

Thermal counterflow in uniform channels exhibits a similar critical heat current corresponding to the laminar-turbulent transition. Whether the transition is from the T-II or the T-I state to laminar flow depends on the size and geometry of the flow channel, but in either case the turbulent state abruptly ceases at some well-defined Q_c, below which only the laminar state is observed. In very long channels, the turbulence has been observed to originate in one location, but such a turbulent-laminar front is not stable, and quickly propagates through the channel.[30] Once the flow reaches a steady state, the entire channel is filled with turbulence. When possible to measure, the

temperature gradient in such long channels has proven to be constant along the channel length, indicating that the turbulent state entered is homogeneous and no stationary turbulent-laminar fronts are present within the channel.

Only in one experiment has a stable and stationary T-II–laminar front been directly observed in a uniform channel, in a flow regime far from thermal counterflow. Over a very narrow range of relative velocities approaching the condition called "co-flow," where $V_n = V_s$ and the average relative velocity $V = 0$, Slegtenhorst, Marees, and van Beelen observed such a stationary T-II–laminar front in one circular glass channel, but not in other channels of comparable geometry.[31] In general, this flow regime exhibits very low dissipation in the turbulent state, since only extremely small line densities can be sustained at such small relative velocities, and displays complex and anomalous behavior that is not as yet well understood.

Restricting our attention to thermal counterflow, the following simple picture of the criterion determining the turbulent-laminar transition is consistent with all uniform channel data. The transition occurs at constant $V_c d$, where d is the narrowest channel dimension. This observation implies that the line density reaches a critical minimum value below which the vortex tangle is not self-sustaining. Using the appropriate model for the T-I or T-II state, as applicable, the line density at V_c can be estimated. A wide range of experiments in uniform channels is consistent with a critical condition of $L^{1/2}d \simeq 2$–3, independent of temperature, and regardless of whether the transition to laminar flow proceeds from a T-I or a T-II turbulent state.[2] Since $L^{-1/2}$ represents the average local radius of curvature of a vortex segment, thinking in terms of the simple geometry of a vortex ring yields the appealing picture that, at $\dot{Q}_c$, a vortex of average size would just "fit" within the channel in any orientation.

For a uniform flow, one cannot truly distinguish which is the more fundamental condition, that V or L reaches a critical minimum value, since these two criteria are essentially synonymous. Our nonuniform channel data offer the possibility of distinguishing between these two conditions. For our diverging flow, $V_c h$ being constant does not correspond to constant $L^{1/2}h$, since the local uniformity approximation does not hold and the local line density is found to be not proportional to V^2. By using the modified line density formula we may predict "isodensity" curves of constant $L^{1/2}h$ by finding, for a given heat current $\dot{Q}$, the location r at which L [Eq. (16)] reaches a value corresponding to the chosen cutoff value of $L^{1/2}h$. This procedure is at best questionable, since it presumes that the modified line density formula accurately characterized the true local average line density at very low heat currents just above the onset of turbulence. We point out that estimating L at V_c from uniform channel data involves a comparable set of assumptions.

Figure 12 displays curves for both constant $V_c h$ and constant $L^{1/2}h$. The value $V_c h = 0.072$ cm^2/s is obtained from $\dot{Q}_c = 0.55$ mW measured at the narrow end of the channel. The isodensity curve of $L^{1/2}h = 4$ was selected as having the best overall agreement with the critical heat current data. Taking all the evidence together, including the inferred $\dot{Q}_c$ at the wide end of the channel, our results clearly favor the interpretation that a minimum $L^{1/2}h$ is the more fundamental criterion. Given the substantial differences apparent in the turbulent states involved, we consider our value of $L^{1/2}h = 4$ to be in excellent agreement with the uniform channel result of $L^{1/2}h \simeq 2.5$.

It is worth pointing out that determining $\dot{Q}_c$ in our nonuniform channel geometry is somewhat more difficult than in a uniform channel experiment for the following obvious reason. Just above $\dot{Q}_c$ in a uniform channel, the entire channel is filled with a low level of turbulence, and the measured signal ΔT is measurably larger than it would be were only laminar flow present. Right at $\dot{Q}_c$ this turbulence vanishes throughout the channel, and a discrete and highly reproducible step can often be discerned between the turbulent and laminar states. By contrast, for any position r in our diverging channel, as $Q_c(r)$ is approached from above the turbulent-laminar front is moving towards r; so very near Q_c most of the flow beyond r is laminar, and only a diminishingly thin slice beyond r is turbulent. As $\dot{Q}$ is decreased, the measured signal ΔT smoothly approaches ΔT_L, as the contribution $\Delta T'$ from this shrinking turbulent slice becomes vanishingly small. The greater difficulty in determining $\dot{Q}_c$ is reflected in the size of our error bars in Fig. 12.

Last, we compare the temperature dependence of $V_c h$ obtained from $\dot{Q}_c$ at r_A with results of two experiments in uniform high-aspect-ratio rectangular channels, the closest uniform analogue to our channel.[19,32] Our results exhibit a monotonic temperature variation similar to these uniform channel data, but our values of $V_c h$ were consistently greater, by as much as a factor of 2. Taken together, the larger $V_c h$ and the agreement with $L^{1/2}h = 4$ suggest that a larger minimum line density is needed to sustain turbulence in a diverging flow than in a comparable uniform flow.

IV. CONCLUSIONS

Our investigations have established that inhomogeneous turbulence in a weakly diverging rectangular channel differs markedly from the homogeneous turbulent state (T-II) observed in uniform channels. The Schwarz model of homogeneous turbulence, so successful in describing the T-II state in uniform flows, when applied in the local uniformity approximation to our nonuniform flow predicts the wrong functional dependence to describe the observed dissipation in the inhomogeneous analog of the T-II state. An even more complicated hydrodynamic model of Geurst, purporting to treat the case of a nonuniform vortex line density existing in a uniform flow, yields predictions that differ only slightly from those of the Schwarz model, and likewise fails to characterize our results.

We achieve a remarkably good parametric fit to our data by severely altering the line density from its expression in the case of uniform flow. Most compelling and most puzzling is the revelation that the modified line den-

sity fitting our data consists of two parts, a local piece (the homogeneous vortex line density rescaled) and a nonlocal piece that does not have any spatial dependence, being a polynomial function only of the drive parameter $\dot{Q}$. The nonlocal piece may therefore be thought of as an average or background line density present throughout the channel. One might argue that this separation of L into two pieces is artificial, just as is any expansion of one function into a sum of other functions. One might therefore caution against assigning too much meaning to the division. This modified line density is, after all, only an "effective" line density — it yields the correct behavior for $T(r)$ upon integration, but L has not been measured directly. We reiterate the point that in the case of homogeneous turbulence in a uniform flow, there is no way to distinguish whether the line density has a solely local character or is comprised of two pieces, one depending on the local velocity and the other constant throughout the channel at any given heat current, since in a uniform flow these two pieces would be indistinguishable.

Our results underscore the need to simulate the vortex line distribution resulting from a nonuniform velocity field. A comparison of the inhomogeneous superfluid turbulent state predicted by direct numerical simulation of our nonuniform flow to our experimental results is needed to determine how and why applying the homogeneous model locally is inadequate to the task of describing our results. Because the functional dependences of the measured dissipation differ so markedly from the predictions of the homogeneous model used in the local uniformity approximation, we suspect that some new contribution to the underlying vortex dynamics must be at work in the inhomogeneous T-II state.

The vortex stretching which necessarily takes place as a vortex filament is transported from one region to another in a nonuniform flow is one mechanism not incorporated in the homogeneous model. The form of the new production term in the line density equation of state resulting from such vortex stretching can be predicted by simple arguments. Unfortunately, the resulting line density does not have the correct functional dependence to agree with our data, but our simple argument does not self-consistently couple the new stretching term to the vortex production present even in a uniform flow, namely, the growth of line length due to the self-induced motion of a vortex filament. While a more careful treatment of vortex stretching might shed some light on the character of inhomogeneous turbulence, we do not believe that vortex stretching contributes significantly to altering the T-II state so dramatically from the homogeneous case.

Also unlikely to account for the difference is any simple adjustment or extension of the parameters in the Schwarz model needed to extend it to nonuniform flow. Although the anisotropy of the tangle may be quite different from that seen in a uniform flow, and the Schwarz parameters might even become more complicated spatial functions, no longer depending solely on the local temperature, it is difficult to see how any extension the homogeneous turbulence model to a nonuniform flow would alter the dependence of the line density on the local velocity drastically enough to agree with our observations.

Recent simulations by Aarts and de Waele exhibit some interesting new features.[12] When they simulate the steady-state line density in a uniform circular channel while constraining the normal fluid cross-channel profile to be parabolic, they find that the vortex line density is largest close to the walls, where the normal fluid velocity (and hence the relative velocity) is low. The spatial variation in the predicted line density exactly compensates for the variation in velocity so that the local mutual friction force, which depends on the product of the local line density L and the *local* relative velocity v, remains essentially constant everywhere except very near the channel walls, where it decreases to zero. For uniform channel flows, the homogeneous model only asserts that $\Delta T' \propto L V$, where V is the cross-channel average of v, and L is constant on statistical average. The Aarts–de Waele simulations seem to suggest that this basic relation is even more robust, holding locally even in situations where L is not constant and does not depend on v^2. The situation they impose is somewhat artificial, in that the normal fluid velocity profile is not allowed to be influenced by the vortex tangle. Nevertheless, their results bear some similarity to our findings, a point which may require closer examination in the future.

According to our modified line density formula, L is much larger than would be predicted by the homogeneous model ($L_h \propto V^2$) at the wide end of the channel, where V is lowest, and correspondingly smaller than L_h at the narrow end of the channel, where V is highest. This situation bears at least a superficial resemblance to the simulation results of Aarts and de Waele, but the similarity may be deceptive. Since the relative size of the local homogeneous piece to the total modified L is a strong function of both position and the heat current, whether the local value of L is dominated by the local homogeneous piece or the nonlocal piece depends strongly on both r and $\dot{Q}$. Thus within some region in our channel, $L \propto V^2$, while elsewhere this relation no longer holds. This situation is quite different from that treated in the Aarts–de Waele simulations, which still pertain to flows that are uniform in the downstream direction.

Last, our data suggest that the laminar to turbulent transition is precipitated by the local velocity reaching a value sufficient to sustain a minimum line density. Unlike a uniform flow, the velocity at which this critical line density is achieved is not itself a constant, because of the complicated dependence of the line density on the local velocity and the underlying drive parameter $\dot{Q}$. A stationary turbulent-laminar front is clearly produced, but many outstanding questions remain about the character of this front. A higher line density is needed to sustain turbulence than is observed in uniform flows. We observe the critical condition to be $L^{1/2}h \simeq 4$, as compared to $L^{1/2}h \simeq 2.5$ for most uniform flows. This observation that the inhomogeneous turbulent state becomes unstable at a higher line density provides another hint towards understanding the underlying vortex dynamics.

One particularly interesting question is whether or not the transition to the T-II state proceeds directly from the laminar state, or is precipitated by a laminar–T-I transition. Since in low-aspect-ratio uniform channels,

the laminar–T-I transition is hysteretic, behaving like a first-order phase transition, but the T-I–T-II transition is continuous, it has always been puzzling why the laminar–T-II transition seen in high aspect ratio channels is hysteretic. The suggestion has been made that the T-I state actually forms first, but for whatever reasons is not stable and gives way immediately to the homogeneous T-II state. One would like to probe the characteristics of the front region itself in a nonuniform flow, since a stationary front can be created and moved at will back and forth within a narrow spatial region. Even if one could achieve extremely good spatial resolution with, for example, two very closely spaced probes, the turbulent temperature signal in the vicinity of $\dot{Q}_c$ is on the same order in size as the measurement fluctuations in the laminar signal. Furthermore, since it is not known how abrupt the T-II/laminar transition ought to be, any information gleaned from even the most careful experimental observations of the front itself would be subject to interpretation as to whether it showed evidence for a small precursor T-I region, or simply a spatially broad transition directly to the T-II state. Much more promising is to experimentally determine only the gross behavior of the transition, such as the $\dot{Q}$ dependence of the front location, and deduce what such easily measured features indicate about the transition to turbulence, based on a theoretical analysis of such transitions.

Future investigations using the same nonuniform rectangular channel will examine the case of converging rather than diverging flow. Although we expect the fully developed turbulent state to be largely unchanged, how the transition to turbulence will be affected by reversing the flow velocity is of great interest. Some significant differences have already been observed in the nature and stability of the front between the cases of diverging and converging flow in a nonuniform circular channel. Interpreting the behavior of these laminar-turbulent fronts is an ongoing focus of present and future investigations. We believe the question of understanding the transition to turbulence is closely linked to that of understanding the observed states of inhomogeneous turbulence, and how and why the inhomogeneous T-II state seen in our nonuniform rectangular channel, and in similar nonuniform circular channels at sufficiently high heat currents, is so different from the state of homogeneous superfluid turbulence.

ACKNOWLEDGMENTS

We are grateful to W. Fiszdon (Polish Academy of Sciences, Warsaw) for helpful discussions at several key stages of this work. This work was supported in part by the National Science Foundation under Grant No. DMR-9107686.

[1] W.F. Vinen, Proc. R. Soc. London, Ser. A **242**, 493 (1957).
[2] J.T. Tough, Superfluid Turbulence, in *Progress in Low Temperature Physics*, edited by D.F. Brewer (North-Holland, Amsterdam, 1982), Vol. VIII, p. 133.
[3] R.J. Donnelly, *Quantized Vortices in Helium II* (Cambridge University Press, Cambridge, 1991).
[4] D.D. Awschalom, F.P. Milliken, and K.W. Schwarz, Phys. Rev. Lett. **53**, 1372 (1984).
[5] K.W. Schwarz, Phys. Rev. B **31**, 5782 (1985); **38**, 2398 (1988).
[6] K.W. Schwarz and J.R. Rozen, Phys. Rev. B **44**, 7563 (1991).
[7] P.J. Murphy, J. Castiglione, and J.T. Tough, J. Low Temp. Phys. **92**, 307 (1993).
[8] K.W. Schwarz, Phys. Rev. Lett. **71**, 259 (1993).
[9] J.A. Geurst, Physica B **154**, 327 (1989).
[10] J.A. Geurst, Physica A **183**, 279 (1992).
[11] J.A. Geurst and H. van Beelen, Physica A **206**, 58 (1994).
[12] R.G.K.M. Aarts and A.T.A.M. de Waele, Phys. Rev. B **50**, 10 069 (1994); R.G.K.M. Aarts, Ph.D. thesis, Technische Universiteit Eindhoven, 1993.
[13] H. Armbrüster and W.P. Kirk, Physica **107B**, 335 (1981).
[14] Y. Maeno, H. Hauke, and J. Wheatley, Rev. Sci. Instrum. **54**, 946 (1983).
[15] D. Griswold, C.P. Lorenson, and J.T. Tough, Phys. Rev. B **35**, 3149 (1987).
[16] M. Yamaguchi, Y. Fujii, M. Kishida, and M. Nakamura, Jpn. J. Appl. Phys. **26**, Suppl. 26-3, 87 (1987).
[17] J.F. Kafkalidis and J.T. Tough, Cryogenics **31**, 705 (1991).
[18] J.F. Kafkalidis, Ph.D. thesis, The Ohio State University, 1994.
[19] D.R. Ladner and J.T. Tough, Phys. Rev. B **20**, 2690 (1979).
[20] R.J. Cornish, Proc. Roy. Soc. London A **120**, 691 (1928); J.D. Henberger, Ph.D. thesis, The Ohio State University, 1982.
[21] S.B. Savage, Trans. ASME J. Appl. Mech. **31**, 594 (1964).
[22] A.F. Elkouh, Appl. Sci. Res. **21**, 284 (1970).
[23] Here $\mathbf{v}$ is used to mean the mass flow of the total fluid and is not to be confused with the local relative velocity $\mathbf{v}_n - \mathbf{v}_s$. In thermal counterflow $\langle \mathbf{v} \rangle = 0$, but $V \equiv \langle \mathbf{v}_n - \mathbf{v}_s \rangle \neq 0$.
[24] S.K. Nemirovskii and V.V. Lebedev, Sov. Phys. JETP **57**, 1009 (1983).
[25] H. van Beelen, W. van Joolingen, and K. Yamada, Physica B **153**, 248 (1988).
[26] In the 1D Geurst model, the direction of $\mathbf{v}_l$ relative to $\mathbf{v}_n$ constitutes an independent parameter which must be specified. Choosing $\mathbf{v}_l - \mathbf{v}$ parallel to $\mathbf{v}_n - \mathbf{v}$ recoups the standard form of the Vinen equation and means that the term involving $L^{3/2}$ behaves as a line production term. This choice, also adopted by Schwarz, is the appropriate one near equilibrium. See the discussions of Eqs. 4-14, 4-16, and also Eq. 3-15ff in Sec. 3 of Ref. 10. The 3D Geurst model generates an additional equation which controls the direction of $\mathbf{v}_l$. In the case of homogeneous turbulence, the 3D model yields stable and metastable solutions for $\mathbf{v}_l$ parallel and antiparallel to $\mathbf{v}_n$, respectively (see Ref. 11).
[27] R.A. Ashton and J.A. Northby, Phys. Rev. Lett. **35**, 1714 (1975); R.T. Wang, C.E. Swanson, and R.J. Donnelly,

Phys. Rev. B **36**, 5240 (1987).
[28] P.J. Murphy, J.T. Tough, and W. Fiszdon, J. Low Temp. Phys. **86**, 423 (1992).
[29] The eighth class (choosing the minus root, $\phi < 0$ and $\gamma_\ell > 0$) also yields a solution L which has a reasonable functional form, but cannot be made large enough in magnitude to fit the data.
[30] S.M. Bhagat, P.R. Critchlow, and K. Mendelssohn, Cryogenics **4**, 166 (1964).
[31] R.P. Slegtenhorst, G. Marees, and H. van Beelen, Physica **113B**, 341 (1982).
[32] E.J. Yarmchuck and W.I. Glaberson, J. Low Temp. Phys. **36**, 381 (1979).